

Review

Current State of Laser-Induced Fluorescence Spectroscopy for Designing Biochemical Sensors

Adam Thomas Taylor and Edward P. C. Lai *

Department of Chemistry, Carleton University, Ottawa, ON K1S 5B6, Canada; adamttaylor@mail.carleton.ca

* Correspondence: edwardlai@cunet.carleton.ca

Abstract: Laser-induced fluorescence (LIF) has been a valuable analytical technique since the 1970s that has only been made more useful through advances in other scientific fields such as biochemistry. Moreover, advances in laser and detector technology have seen a decrease in LIF detector costs and an increase in their ease of use. These changes have allowed for LIF technology to be widely adopted for various sensor designs in combination with advanced instruments. With advances in biochemistry necessitating the detection of complex metabolites, labelling with fluorescent chemical reagents may be necessary to improve detection sensitivity. Furthermore, advances made in fluorescent labeling technologies have allowed for the use of LIF in the detection of nanoparticles as well as for imaging techniques using nanoparticles as signal amplifiers. This technology has become invaluable in the detection of environmental pollutants, monitoring of biological metabolites, biological imaging, and cancer diagnosis, making it one of the most valuable analytical science techniques currently available.

Keywords: laser-induced fluorescence; aptamer; biochemical agents; fluorescence detection; metal oxide nanoparticles; sensor design



Citation: Taylor, A.T.; Lai, E.P.C. Current State of Laser-Induced Fluorescence Spectroscopy for Designing Biochemical Sensors. *Chemosensors* **2021**, *9*, 275. <https://doi.org/10.3390/chemosensors9100275>

Academic Editor: Xiaobing Zhang

Received: 4 August 2021

Accepted: 20 September 2021

Published: 27 September 2021

Publisher's Note: MDPI stays neutral with regard to jurisdictional claims in published maps and institutional affiliations.



Copyright: © 2021 by the authors. Licensee MDPI, Basel, Switzerland. This article is an open access article distributed under the terms and conditions of the Creative Commons Attribution (CC BY) license (<https://creativecommons.org/licenses/by/4.0/>).

1. Introduction

Laser-induced fluorescence (LIF) spectroscopy is a technique that can empower a chemical analysis laboratory to easily monitor the concentration of inherently fluorescent compounds and enable the development of new analytical methods that utilize fluorescent labeling [1]. Fluorescence detection functions by shining light on a sample at the analyte's optical excitation wavelength and collecting the light from the analyte at its emission wavelength perpendicular to the incident beam. The incident beam can be produced from a variety of sources including lasers, light-emitting diodes, tungsten-halogen bulbs, and arc lamps (containing mercury, xenon, or deuterium). These light sources have their own advantages and disadvantages, and the intended use of the detector dictates which source can be used [2]. LIF spectroscopy offers several advantages over absorption spectroscopy. First, LIF has excellent detection sensitivity because a signal is observed against a dark background. Second, the emitted radiation can be collected at various angles with respect to the collimated laser beam, making it possible to obtain two- and three-dimensional images. Third, LIF imaging of translucent and opaque materials is particularly attractive due to the strength of the resonant absorption process compared with the non-resonant Rayleigh techniques in Raman spectroscopy. Fourth, by dispersing the fluorescence, it is also possible to learn about the transitions from the excited state to various lower energy levels of the fluorescent molecule. Fifth, because of the delay between the excitation and detection events, it is possible to study the processes the excited molecule undergoes in the intervening time [3]. This technology has seen many improvements and novel uses over the last couple of decades. As new LIF-based research and applications rise in number every year [4], the justification for any science or engineering laboratory not having an LIF detection system continues to dwindle. A pioneering LIF application can be found in the early work by Hofzumahaus and Holland, wherein the measurement of tropospheric OH radicals achieved a detection limit of $8.2 \times 10^6 \text{ } \bullet\text{OH}/\text{cm}^3$ [5]. Ambient air was expanded

through a nozzle into a fluorescence cell and irradiated by a pulsed frequency-doubled dye laser. The laser wavelength was tuned to selectively excite the $\bullet\text{OH}$ radicals on a single rovibronic transition at 308 nm. The OH-resonance fluorescence, emitted mostly between 307 and 311 nm, was detected by a gated photomultiplier/photon counter assembly.

As synthetic biochemistry and biomedical engineering make scientific advances, there has been a growing need for sensitive methods of detecting biological metabolites, proteins, endoplasmic reticulum membranes, living cells, cancers, and organelles [6–9]. Most tissues contain several different fluorescent compounds, which include the amino acid tryptophan, the oxidation-reduction mediator NADH, the connective components elastin and collagen, porphyrin, as well as pyridoxal acid. However, the amounts of fluorophores are different between normal and abnormal tissues. Their unenhanced autofluorescence patterns seem capable of detecting neoplasms [10]. Quantitatively, LIF is a powerful tool widely used in glycan analysis with fluorophore-labeled carbohydrates where each species has a common response factor. Electrospray ionization mass spectrometry (ESI-MS), on the other hand, while revealing important structural information about individual analytes, generally have different response factors for the quantitative analysis of different species. For improved quantitation with ESI-MS, laser-induced fluorescent images were collected at the Taylor cone of the electrospray interface, enabling simultaneous optical quantitative optical and qualitative MS detection of fluorophore-labeled sugars. The limit of LIF detection was 40 attomoles; the intra- and inter-day peak area reproducibilities were 4.2% and 6.8%, respectively [11]. Furthermore, the need extends to the detection of environmental contaminants that have been found in foods through processing and packaging activities. Fluorescence detection is a popular technology of detecting contaminant molecules, as many are either inherently fluorescent or can be made to be fluorescent through labeling [12–15]. This technology is also popular for its cost effectiveness compared to other advanced technologies like mass spectrometry [16]. In addition, fluorescence detection does not suffer some of the issues that affect mass spectroscopy, such as the inability to distinguish between molecules (or fragments) with identical mass-to-charge ratios without capital investment on high-resolution mass spectrometers, difficulty with ionizing samples to form molecular ions, and complicated troubleshooting that mass spectrometry instrumentation can cause [16,17]. Furthermore, mass spectrometry is not necessarily the best available technique for virological analysis because of the time-consuming and tedious image collection process. LIF is applicable to the visual classification of viruses, reducing the time and costs for this analysis. Rossi et al. performed experimental tests in which different viruses were irradiated with a UV laser beam at 266 nm and the emission spectra were recorded by a spectrometer. Their classification techniques demonstrated the feasibility of discriminating viruses. The development of a rapid virological analysis allows fast responses to epidemiologic events, thus reducing their risks to public health. Moreover, a cost reduction translates to an increase in the number of sampling sites monitored, with potential enhancement of prevention and control of disease spread [18]. All these scientific papers contributed towards the ever rising number of LIF publications, based on the yearly statistics retrieved from Google Scholar between 2001 and 2021, as shown in Figure 1.

In this review, the development of LIF detector technology for biological, catalytic, chemical, environmental, enzymatic, radiological and toxicological sciences since 2010 is described. Detection system designs are classified based on the excitation light source, molecular probes/tags [19,20], sample cell configuration, and electrooptical detector specifications. Advanced technologies of laser-induced breakdown spectroscopy (LIBS) and spectrometers based on cutting-edge quantum cascade (QC) and interband cascade (IC) lasers are accounted for a comprehensive review.

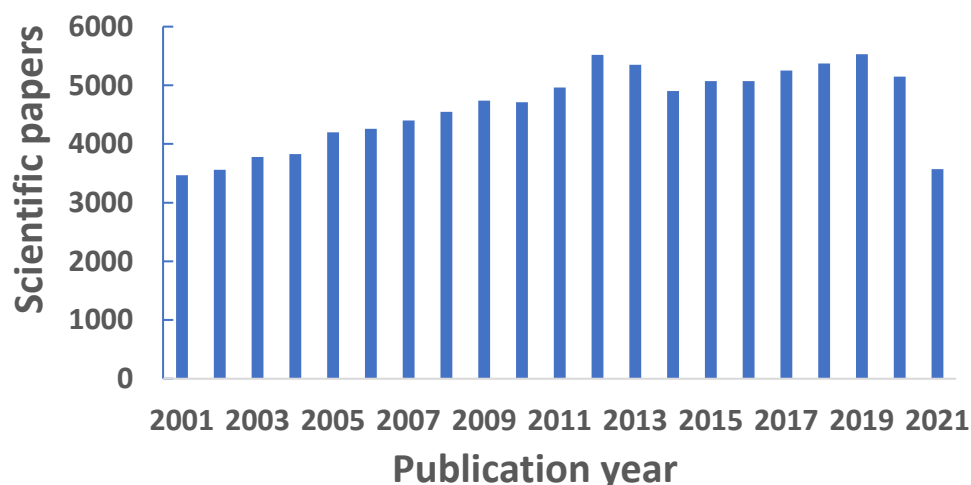


Figure 1. Yearly statistics of scientific papers published between 2001 and 2021 in the research area of laser-induced fluorescence.

2. Designing a LIF Detection System

LIF is a method of choice for real-time field screening of residual organic contaminants in ground water, undisturbed vadose, capillary fringe, and subsurface soils. The technology is intended to provide highly detailed, qualitative to semiquantitative information about the distribution of subsurface contamination that fluoresces, such as petroleum products containing polycyclic aromatic hydrocarbons (PAH) [21]. Detection systems based on LIF can be custom built in the laboratory from commercially available components that meet the specific design needs of the researchers. Three-dimensional printed parts can be used in conjunction with these components to significantly reduce costs and construction time of the bench-top system [22]. NASA has built a high-performance LIF instrument for the detection of airborne formaldehyde [23]. Rotational-state specific excitation at 353 nm is achieved by using a compact fiber laser (10 mW output power), with a single-pass design for stable signal response and a stand-alone data acquisition system. The accuracy of reported mixing ratios of tropospheric formaldehyde is $\pm 10\%$ based on calibration against IR and UV absorption of a primary HCHO standard. Precision at 1 Hz is typically better than 20% above 100 parts per trillion by volume (pptv), with uncertainty in the signal background contributing mostly to variability at low mixing ratios. The detection limit (for a signal-to-noise ratio of 2) is 36 parts per trillion (ppt), and the time response at typical sample flow rates is 0.19 s [24].

An instrument was designed for LIF detection of NO_2 to determine the peroxy nitrates, alkyl nitrates, hydroxyalkyl nitrates, and HNO_3 total, attaining a detection limit of 90 ppt in field observations [25]. A single-photon LIF sensor was recently developed for atmospheric measurements of nitric oxide (NO) in the atmosphere. Rapid tuning of a narrow-band laser on and off of a rotationally resolved NO spectral feature near 215 nm and detection of the red-shifted fluorescence provides for interference-free direct measurements of NO with a detection limit of 1 pptv for 1 s of integration, or 0.3 pptv for 10 s of integration. The instrument has been deployed on the NASA DC-8 aircraft and provided more than 140 h of NO measurements over 22 flights autonomously [26]. Analysis of dissolved organic matter (DOM) concentration and composition is essential for quantifying biological and chemical oxygen demand in natural waters; however, manual water sampling is costly and time consuming over large areas. An airborne LIF light detection and ranging (LiDAR) system was designed to assess the DOM concentration of the Annapolis River and Basin (Nova Scotia, Canada) as well as three rivers and their estuaries (in Prince Edward Island, Canada). Two flight missions were conducted in the summers of 2008 and 2009 and positive correlations were found with traditional sample collection [27].

Fluorescent PAH molecules may be contained in non-aqueous phase liquids (NAPLs) including petroleum fuels/oils, coal tars, and creosotes. Direct push logging of the inherent

fluorescence of an NAPL with depth provides rapid and cost-effective delineation of NAPL. A clear sapphire window is fitted into the side of a direct probe that is pushed through the soil column. As this sapphire-windowed probe is advanced steadily into the soil column at approximately 2 cm/s, pulses of laser light are sent down via fiber optics to exit the window and shine onto the passing soil. Any resulting fluorescence that comes back into the window is brought up by a second fiber for data processing and analysis in real time. LIF systems can log up to 30 m below the ground surface, taking approximately 45 min from start to finish [28].

There is always a need for forensic laboratories to conduct evidence analysis in a post blast scenario. The development of portable sensors for fast screening of crime scenes is required to reduce the number of evidences useful to be collected, optimization of time and resources. A multispectral LIF imaging system is able to detect evidence of different materials on very confusing areas at distances up to tens of meters. A short analysis time, but with sufficient accuracy of forensic evidence at the original crime scene, was a main requirement in the system design. Plastics (polypropylene, polyethylene and polyester) were identified and their locations in the examined area were highlighted through data processing. By proper choice of emission bands, the LIF imaging system can be used for the rapid detection of other material classes (textiles, woods, and varnishes) [29].

The capsid protein purity of adeno-associated virus (AAV) is considered a critical quality attribute of gene therapy products. However, the viral capsid proteins are present in extremely low concentrations. A one-step denaturation and fluorescence labeling procedure for AAV capsid proteins (using the Chromeo™ P503 dye) enabled the establishment of a capillary electrophoresis-sodium dodecyl sulfate method with LIF for AAV detection. The method has been validated to be accurate and precise with a linear dynamic range of 8.0×10^7 – 3.0×10^{11} vector genomes per mL (vg/mL). The detection limit and quantitation limit were established to be 8.0×10^7 vg/mL and 4.2×10^8 vg/mL, respectively [30]. LIF is also a very sensitive detection method in micro total analytical systems (μ TAS) owing to the good monochromaticity, strong collimation and high optical density of diode-pumped solid-state lasers. Due to its important role in μ TAS, different optical structure arrangements of LIF detection have undergone continuous development [31].

3. Excitation Light Sources

Arc lamps are the most popular light sources used in fluorescence detectors [32]. Arc lamps, like other lamps, have the advantage that they offer a wide spectrum, which can be separated by a monochromator to allow one lamp to be used in a variety of fluorescence applications [33]. Arc lamps function by using high voltages to form a sustained arc of electrons between two plates [34]. The gas that is used to facilitate the arc of electrons is what gives the lamp its spectrum, as well as determining the stability of said spectrum [33].

Unlike arc lamps, tungsten–halogen bulbs function by passing electricity along a wire of tungsten in the presence of a halogen gas [35]. This causes the tungsten to heat up and release gaseous tungsten, which then reacts with the halogen, producing light, before redepositing the tungsten onto the wire [36]. As the tungsten of these lamps needs to reach very high temperatures in order for it to function, they do not have a very long life compared to other light sources [37].

Light-emitting diodes (LEDs) are a light source of growing popularity owing to their comparatively small size and low cost [38]. Unlike previously described lamps, multiple different colored LEDs are required in a fluorimeter in order to cover the same wavelengths emitted by a lamp [39]. LEDs function by using running electricity through a semiconducting material (e.g., GaAs), which causes electrical holes to be filled, releasing energy as light [40]. Additionally, the intensity of light offered by conventional LEDs is low compared to available lasers, despite both having similarly narrow spectra [41].

LIF is one of the most sensitive detection methods. Lasers were first utilized in fluorescence detectors in 1968 when Richard Zare used a He-Ne laser to perform spectroscopy on gas-phase potassium molecules [42]. Laser light offers many advantages not possible

with the other above-mentioned sources. Firstly, unlike lamps and LEDs, lasers produce thin beams of light with photons moving in the same direction, and thus do not diminish in intensity as quickly as other light sources [43]. This allows for a longer distance covered between the light source and sample without losing excitation light intensity by the inverse-square law [44]. Furthermore, like LEDs, lasers offer a very small selection of wavelengths in the output beam, which negates the need for a monochromator which is necessary when using arc lamps [45]. Moreover, lasers can also be pulsed at very high frequencies to apply higher intensity light as compared to continuous wave lasers, but at a frequency such that the fluorophore can relax to its ground state before being excited again [46]. However, this higher light intensity can cause photodegradation, which can negatively impact sensitivity as the fluorophore molecules are degraded [46,47].

LIF is an important technology for the detection of organic molecules as well as minerals on the surface of Mars [48]. Frequency multipliers of the Nd-YAG laser output (1064 nm) produce harmonic wavelengths that are suitable for fluorescence excitation of perchlorate (at 355 nm) and PAH (at 266 nm and 355 nm but not 532 nm) [48]. A LIF-based detection system was evaluated for the influence of time-resolved data on the biological agent classification accuracy. A multi-wavelength sub-nanosecond laser source was used to acquire spectral and time-resolved data from a standoff distance of 3.5 m from seven different bacterial species and six types of oil. Classification performed with a decision tree algorithm showed that accuracy was increased from 86% for spectral data only to more than 92% when combined with time-resolved data [49].

As real-time detection and monitoring of microbial contamination on solid surfaces is mandatory in a range of biomedical, safety and security applications, a LIDAR device was designed using the LIF method based on dual wavelength sensing with multispectral pattern recognition system. Microbial simulants (bacteria, bacterial spores, fungal conidia and virus) were assessed and the spectra of dead versus living *E. coli* showed differences at various sensing wavelengths [50].

A variant of LIF imaging of increasing interest is multiphoton microscopy. This technique uses IR rather than visible or UV light in order to excite fluorophores [51]. This is possible as the sum of the energies of the two (or more) IR photons (often of different energy) used can excite the fluorophore [52]. While this would convolute LIF detection, it is preferred in imaging as IR light penetrates tissues deeper than visible and UV light [53]. Moreover, the use of two IR photons excludes all fluorophores other than the target that will fluoresce. It allows for multidimensional imaging, as two laser excitation beams must cross at a spatial point to induce fluorescence [54].

4. Molecular Probes/Tags

As not every molecule is highly fluorescent, especially under visible light, molecules must be labeled with fluorescent tags in order to detect them [55]. A wide selection of fluorescent tag products are commercially available, including labeled antibodies and conjugates, as well as reactive dyes and labeling kits. Over thirty reactive dyes have been synthesized for LIF applications across the visible, far-red and near-IR spectra. Their high performance offers superior brightness, photostability, and solubility [56].

The most notable examples of LIF applications in biology is tagging proteins with green fluorescent protein (GFP) and its many derivatives [57]. Many proteins can be tagged with this protein by adding a DNA sequence encoding GFP in frame with the protein to be tagged; the resultant fusion protein will be fluorescent, with minimal impact on protein function [58]. Other common dyes such as fluorescein, rhodamine, and various Alexa Fluors must be chemically bonded to their targets, which makes them only viable when labeling can be done outside a biological system [59–61]. When this technology is applied to antibody labeling, cells and tissues can be fluorescently labeled based on the expression of a target protein [62]. Antibody labelling can be invaluable in the research of drug delivery vehicles, as their path to the target tissue can be monitored [63]. This

can allow researchers to modify their targeting methods or delivery vehicles based on the results from the fluorescence experiments.

In addition to conventional fluorophore labeling, advances in nanoscience have allowed for LIF labeling with fluorescent nanoparticles called quantum dots (QDs) [64]. QDs are nanoparticles made of semiconducting materials whose size and material composition dictate its fluorescence properties [65]. The mechanism of QD fluorescence differs from conventional fluorophores as they utilize quantum confinement in order to create bandgaps that produce fluorescence [66]. Quantum confinement occurs when the diameter of a nanoparticle approaches the de Broglie wavelength of the electron wave function [67]. A potential well is formed, and the band gap becomes proportional to the particle size [68]. QDs have several advantages over more conventional probes, mainly their high quantum yield, broad absorption spectrum, narrow and size-tunable emission wavelengths, as well as superior durability especially to photobleaching [69].

QDs can be categorized into three types: core-type, core-shell, and alloyed [70]. Core-type QDs can be distinguished by the fact that they are composed of a single material, such as CdTe [71]. Core-shell QDs are distinguished from core-type as they contain two distinct layers of semiconductors, with the outermost layer having a higher band gap than the core [72]. Core-shell QDs have several advantages compared to core-type QDs, most notably their increased quantum yield, stability, and adjustable wavefunction engineering [73,74]. Alloy-type QDs, like core-shell QDs, consist of two different semiconductors; but rather than being in distinct layers, they are alloyed together, forming a homogenous nanoparticle [75]. These QDs are easier to produce than core-shell QDs and offer similar advantages over core-type QDs [76]. In addition to being distinct types, they can be combined into QDs with distinct layers, one or more of which are alloyed [77].

As most QDs contain cadmium and another heavy metal, they pose some risk of heavy metal poisoning when introduced into the body; thus there has been growing interest in less toxic forms of QDs for use in imaging [78]. Some examples of QD semiconductors which contain comparatively less toxic heavy metals are InP, CuInS₂, Ag₂S, ZnS-AgInS₂, silicon, and graphene [79]. These materials, although less toxic than CdTe, do have some toxicity, thus requiring extensive toxicity tests before they can be approved for medical use [80].

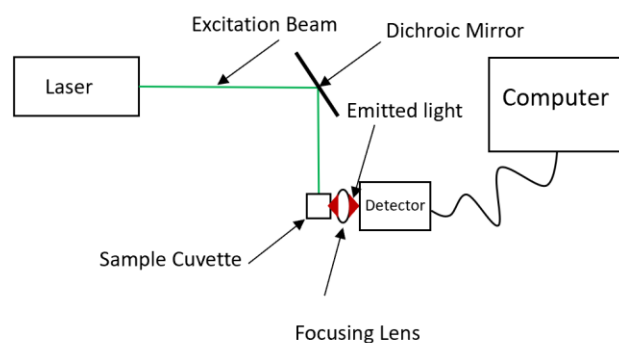
In addition to the fluorophore action that QDs provide, nanostructures such as nanoparticles and nanorods can also serve to quench the fluorescence of other fluorophores [81]. This can be useful as a method for the detection and imaging of compounds that would otherwise have low fluorescence intensity due to the molecular properties or a low fluorophore concentration. However, the use of nanostructures can increase their intensity [81] or produce a higher fluorescence output in imaging [82]. In addition to the more common metal or metal oxide nanoparticle enhancement, research has also shown that carbon-based nanoparticles show similar enhancement, which could prove to be useful, and as such nanoparticles may be more suitable for use in vivo compared with other nanostructures [83].

The most logical application for these fluorophores is in combination with targeting molecules such as antibodies and aptamers [84]. This can be seen in Santana et al., in which researchers were able to attach a ZnS-AgInS₂ QD to an anti-vascular endothelial growth factor (VEGF) receptor antibody [85]. The goal of this was to target brain cancer cells so that the tumors could be imaged and treated by blocking VEGF receptor activity with the antibody conjugate [85]. Results showed a statistically significant decline in cell viability of U87 cancer cells tested compared to the HEK 293T cell control [85]. Other research by Dobhal et al. focused on imaging of exosomes, vesicles released from cells, as they are useful as biomarkers [86]. Specifically, by attaching an InP-ZnS QD-anti-CD63 antibody conjugate to CD63 (a protein known to be expressed on the surface of exosomes), the authors were able to image the exosomes for use as biomarkers of complex cell processes [86].

5. Sample Cell Configurations

Two common optical geometries, as shown in Figure 2, can be constructed for LIF detection—an orthogonal design and a collinear design, for collection of fluorescence. Using Cy5.29 dicarbocanine dye, a limit of detection (LOD) of 7.4×10^{-11} M was obtained using the orthogonal geometry and 1.2×10^{-12} M using the collinear geometry [87]. Latest advancements have resulted in a significant increase in sensitivity to achieve a signal noise ratio of 2300:1 based on the water Raman peak [88]. Capillary electrophoresis (CE) can be coupled with sheath-flow LIF detection to offer outstanding sensitivity for biochemical analysis. In CE-LIF, a plug of sample is electrophoretically driven down a fused silica capillary by applying a high voltage between the inlet and outlet ends. Molecules of different sizes and charge states travel at different velocities down through the narrow capillary channel. However, a major drawback remains with the complexity of the traditional optical configuration. Confocal LIF detection in CE analysis can be simplified using fiber optics and micro gradient-index lenses for modular optical design with a sheath-flow cuvette. The system performance affords a concentration detection limit of 8 ± 2 pM and mass detection limit of 57 zeptomoles for sodium fluorescein [89].

Orthogonal LIF Detector



Collinear LIF Detector

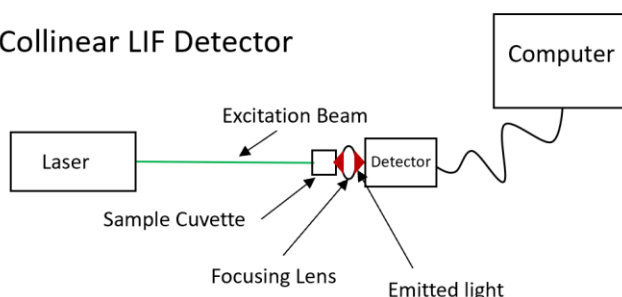


Figure 2. Simplified designs for orthogonal and collinear LIF detector arrangements.

Microfluidic chips/devices for CE analysis were conventionally constructed with LIF detection in an orthogonal optical arrangement. Sensitive detection could be achieved by detecting the fluorescence light emitted in the microchannel through the sidewall of the chip to reduce background noise due to scattered light from the excitation beam. A fluorescence collection angle of 45 degrees in the chip plane could yield better signal-to-noise ratios as the scattered light intensity decreased to only 1/38 of that obtained at an angle of 90 degrees. A detection limit ($S/N = 3$) of 1.1 pM fluorescein was obtained, which is comparable to that of optimized confocal LIF systems [90]. Microfluidic CE has the potential to analyze single cells. However, detection at the low concentration limit of biological dynamic range involves coupling the fluorescence into confocal set-ups using externally cooled photomultiplier tubes (PMTs). The integration of photodetector elements directly on-chip is desirable. A LIF detection scheme embedded a high refractive index micro-ball lens in a

carbon-blackened polydimethylsiloxane panchromatic filter. The lens-filter layer enables simultaneous excitation rejection and fluorescence enhancement to couple fluorescence from a microfluidic channel to a surface photodetector [91]. A strategy combining minimal system design and low-cost system construction was adopted to achieve instrumental miniaturization. The total size of the microfluidic CE-LIF bioanalyzer was minimized to 90 mm length \times 75 mm width \times 77 mm height and the instrument cost was reduced to USD500. After attaining a detection limit of 1.0 nM sodium fluorescein, this bioanalyzer was applied to colorectal cancer diagnosis by the polymerase chain reaction-restriction fragment length polymorphism method [92]. Another LIF detector was developed for pesticide residues based on a microfluidic sensor array, utilizing a spectral recognition method for unsupervised pattern recognition to analyze the characteristic fingerprint-like fluorescent spectral patterns [93]. The detector system responded to pesticide concentrations of 10 ppb [93].

Beam divergence at the exit end of the first optical fiber attenuates the power density of optical excitation, and coupling at the entrance end of the second optical fiber makes it inefficient to collect the fluorescence light from a microfluidic chip. The excitation power and coupling efficiency can be significantly increased by using an on-chip micro-lens system with integrated optical fibers, specially designed by Code V[®] lens design software [94]. Numerical simulations can be conducted to optimize the distance between all optical elements. The micro-lens was produced using direct lithography of SU-8 photoresist [94]. The emitted light can be collimated by an objective and passed through a variety of optical filters in order to increase the spectral selectivity of the detection method [4,94,95]. A modular microfluidic CE system with LIF detection was constructed to analyze amino acids (valine, serine, alanine, glycine, glutamic acid, and aspartic acid) in borate buffered solutions at concentrations ranging from 10 mM to 50 mM (pH 9.5). Among them, the 35 mM borate buffer generated the highest resolution before Joule heating dominated. The limits of detection for alanine and glycine were determined to be 2.1 nM and 2.9 nM, respectively [96].

6. Electrooptical Detector Technologies

Usually, LIF systems are constructed in research labs to detect chemical analytes in biological samples, using a low-power continuous-wave laser as the excitation source. However, as the luminosity of emitted light is often very low, methods of amplifying the signal are necessary [97]. The most common method used to amplify low luminosity light signals into an electric signal is the photomultiplier tube (PMT) [98]. When photons interact with a series of dynodes of an increasingly positive potential within the vacuum tubes in a PMT, electrons are being ejected, which will then be multiplied, producing a 100-million-fold increase in signal strength [99], resulting in an exponentially amplified signal [100].

There have been several advances in PMT technology since their development by Kubetsky in 1930 [101,102]. One of the first such advancements was the development of the avalanche photodiode (APD) in the 1950s by Nishizawa [103]. An APD differs from a PMT in that the former utilizes a single amplification event in a diode, which allows the detector to be significantly smaller, but at the cost of signal-to-noise ratio [104]. As a result of their very small size compared to PMT, APD are very commonly utilized in optical fiber based detectors [105].

The most significant advancement was the development of silicon photomultipliers (SiPM) [106]. SiPMs are a combination of APD and PMT, where the electrons are multiplied similarly to an APD but amplified similarly to a PMT [107]. This difference leads to a more compact, cost effective, and resilient tool that uses lower operating voltages [108].

Two single-mode optical fibers can be framed up in a V-shaped configuration for transmitting the excitation light and detecting the induced fluorescence to construct a scanning LIF detection system for microfluidic CE analysis [109]. Ultra-compact spectrometer modules based on proven diffraction grating technology can be purchased for

spectral resolution of emission wavelengths across the visible to near-infrared range. These spectrometers offer a cost-efficient module for both independent researchers and Optical Emission Spectroscopy manufacturers of analytical instruments, who do not want to sacrifice performance and robustness for compactness [110]. Either a PMT, charge coupled device (CCD), or APD can be used as the detector. A high-speed APD provides responsivity between 400 and 1000 nm, as well as extremely fast rise and fall times at all wavelengths. The responsivity of the device is independent of modulation frequency up to about 800 MHz. The detector chip is hermetically sealed behind a flat glass window in a modified TO-18 package, affording a useful diameter of 0.5 mm as the photosensitive surface. It is also packaged in a TO-18 lightpipe, which allows efficient coupling of light to the detector from an optical fiber up to 0.25 mm in diameter [111]. The detector output signal is acquired by a current-to-voltage conversion circuit, amplifying circuit, and peak-holding circuit. The digital peak signal can then be processed by a computer [44].

A virtual instrument system based on LabVIEW was reported for the design and operation of LIF detection. This system achieves synchronous control of equipment and acquisition of real-time fluorescence data by communication with a computer via GPIB, USB, RS232 and parallel ports. It can perform sequences of operations automatically to obtain the excitation and emission spectra. The system opens up new possibilities for researchers and increases the efficiency of complicated operations of functional components at the click of a button in LabVIEW. The authors will provide a copy of the virtual instrument system upon request [112].

7. Commercial Availability of LIF Detection Systems

When the LIF technology was initially developed, the instruments were manufactured in laboratories [113]. When the technology was growing in popularity in the 1970s, it was very difficult to incorporate lasers in commercially available LIF detectors at the time [114]. However, with the advent of viable lasers, commercial LIF detectors were put on the market by several leading scientific instrument companies.

The SCIEX 800 Plus pharmaceutical analysis system comprises a 488-nm laser module with an output power of 3 mW. With LIF detection, low fluorescence emission light intensities are measured against a dark background. These intensities are easily influenced by changes in the optical path. Due to this uncertainty, LIF detector response is annotated in relative fluorescent units (RFU). A calibration is performed to correct for these changes by using fluorescein (1×10^{-7} M in water). The LIF detector system is designed to guide the fluorescence emission light via a fiber optic cable to the photomultiplier detector. Flashlight can be used to verify fiber optic output. To check noise, drift and baseline stability, fluorescein solution is run with laser off for 5 min followed by laser on for 5 min. A flat baseline with a small step increment of RFU at 5 min should verify good operation of LIF [115].

Planar LIF is an optical imaging technique based upon fluorescence emitted from chemical species excited by planar laser light to measure instant whole-field concentration or temperature maps. Essentially a sheet of laser light is passed through a flow field, and the subsequent fluorescence emission is captured on a 2D CCD imaging sensor, imaging fiber optics, or time-gated digital camera to acquire spatial information. Planar LIF can be used for a range of concentration, pressure, temperature and velocity measurements in different liquid and gaseous flow environments. Current applications are found in sprays, combustion diagnostics, flame radicals, process engineering, biomedical engineering, and fluid mechanics/dynamics research [116]. In studies involving mixing of fluids, one of the fluids is marked with the dye tracer compound, whereas the other is fresh fluid. A laser light sheet illuminates a thin plane in the flow and the tracer absorbs some of the excitation light to emit fluorescence. Commonly used dyes for measurements in liquids are rhodamine 6G (for concentration measurements), rhodamine B (for temperature measurements). Commonly used tracers for measurements in gas phase flows are ketones such as acetone. A camera equipped with a sharp cut-off or narrow-band filter is used

to record only the fluorescence light [117]. For pulsed UV LIF applications usually an image intensifier amplifies the LIF signal. The conversion of LIF images into meaningful concentration or temperature fields is based on calibration measurements.

CE coupled to LIF detection offers a highly specific method with exceptional sensitivity for the analysis of proteins, peptides or glycans. Detectors from Picometrics Technologies SAS (Toulouse, France) can be combined with the Agilent 7100 CE seamlessly. Picometrics ZetaLIF detectors are ultra-sensitive solutions for all separation techniques such as liquid chromatography (capillary, micro, nano, or ultraperformance) and CE. This detector enables an unrivalled level of sensitivity for LIF measurement owing to a broad range of lasers (offering an excitation wavelength from 266 nm to 785 nm) and a wide variety of filter blocks for selecting an optimal emission wavelength [118]. Due to the fiber optics approach used by Picometrics detectors, LIF analysis can readily be combined on-line with any Agilent CE/MS instrument to deliver CE-LIF-MS data. This system combines the power of highly sensitive LIF detection with identification (or structure analysis) of compounds delivered by mass spectrometry [119].

8. Modern LIF Technologies

There have been several advances in LIF technology since their inception in the 1970s. One of the most notable improvements came with the advances in laser diode (also referred to as semiconductor lasers) technology [120]. The first laser diodes were bulkier, less powerful, and did not operate well at room temperature as compared to more modern diodes [121]. These advancements have made diode lasers both cheaper and smaller compared to more conventional gas laser technologies [122].

In addition to the advancements in diode technology, the use of fiber optics has also been a great improvement to LIF technologies [123]. Optical fibers use total internal reflection along a very thin glass conduit of high-refractive index (>1.480) as a waveguide in order to transport light signals across large distances without losing signal strength [124]. Due to the waveguide mitigating any significant loss of light intensity that occurs over long distances of propagation, lower intensity fluorescence can be detected [125]. Optical fibers are commonly implemented into fluorescence detectors either after the light source, before the detector, or both [126]. Designs that implement optical fibers do offer distinct advantages over those that do not, although there are disadvantages that prevent them from being used in every system. Most notable of these disadvantages are the increase in cost compared to systems that do not use fiber optics, and the fragile nature of these glass fibers if not physically protected by a cladding [127,128]. However, when implemented properly, optical fibers allow for distinct separation of both the light source and detector from the sample, allowing for less stray light in a compact design [129].

In addition to advances in available parts, other advances in technology, especially separation technologies, have necessitated integration with LIF detection [130]. Common technologies include, but are not limited to, high-performance liquid chromatography, CE, microfluidics, and flow cytometry [131–135]. Most of these integrations simply involve the replacement of a standard cuvette with a flow cell (or in the case of CE, a section of optical window along the capillary) after the separation [136]. However, this is not the only way to do it, especially when improvements like sheath flow hydrodynamic focusing is adapted [137].

9. Sensors (Site Characterization and Analysis Penetrometer System)

Site Characterization and Analysis Penetrometer System (SCAPS) is a cone mounted sensor developed in the 1990s for use in detecting soil contamination [138]. The sensor, which contains an LIF detection system, must be inserted into the ground, and then volatile soil contaminants can diffuse through a membrane incorporated in the device, where they can be detected by LIF [139]. A hydraulic system can be truck-mounted on these sensors to facilitate real-time chemical measurements. It is best used for screening petroleum hydrocarbon compounds in soil/water and monitoring the performance of PAH

cleanup [140]. A compact spectrometer used 405 nm excitation to acquire LIF spectra in the 450–930 nm spectral range on a solid surface via an optical-fiber coupled measurement head. The prototype instrument was successfully tested on biological soil crust for the detection of chlorophyll at concentrations down to 5 ng/cm² [141].

10. Laser-Induced Breakdown Spectroscopy

In recent years, LIBS has been widely used in many fields of scientific research for chemical element detection. In LIBS, a sample is excited with intense laser pulses and the emitted light is analyzed, which generally falls in the visible or infrared spectral region. LIBS is ideal for sample analysis as it does not require sample preparation, and generally removes less than 1 µg of material during laser ablation [142]. LIBS is fast, causes little sample damage (ablation crater radius < 70 µm), can be applied on-line, and applicable in remote field locations [143]. The LIBS plasma (or ablation vapor plume) was produced by a Q-switched Nd:YAG laser at 1064 nm, and the resultant radiation was detected using a Paschen–Runge spectrometer equipped with photomultipliers [144]. The photomultiplier signals were processed by a fast gateable multichannel integrator for the simultaneous analysis of different elements [145]. LIBS is often combined with molecular LIF to study plasma-borne molecules [146]. The experiments are normally performed in air at atmospheric pressure. When excited by a nanosecond optical parametric oscillator laser tuned at 283.31 nm, emission from Pb atoms was then observed at 405.78 nm with a detection limit of 180 ppb over 100 laser shots. In the double pulse resonant LIBS system, a wavelength-tunable laser was divided into reflection and transmission beams by using a beam splitter. The reflected laser pulse was firstly used to ablate the sample, and then the transmission laser pulse was used to resonantly excite the target atoms in the vapor plume [147]. Femtosecond LIBS for in situ ammonia (NH₃) measurements was demonstrated when a femtosecond laser beam ($\lambda = 800$ nm) was focused at NH₃ molecules, photolysis generated electronic-excited NH fragments with subsequent fluorescence detection at 336 nm to attain a lower limit of 205 ppm [148]. Data from single-line LIBS for seven major rock-forming elements (Al, Ca, Fe, Mg, Si, Na and K) were collected to produce pseudo-logs of geochemical data that are representative of stratigraphy [149]. The optimal LIF excitation locations were the center of the plasma for Fe, but the periphery for Cr and Ni. By focusing an excitation laser beam at the optimal locations, not only excitation efficiency, but also the accuracy of quantitative LIBS-LIF analysis, were improved compared to those with excitation at the plasma center in conventional LIBS-LIF [150]. Ground-state Co atoms in LIBS plasma were resonantly excited by a tunable laser at 304.40 nm. The LIF detection limit was 0.8 µg/g in steel matrix [151]. LIBS-LIF was validated to enhance the spectral intensity of uranium in ores and eliminate spectral interference. In contrast with atomic lines, uranium ion lines are more suitable for determination of uranium. A detection limit of 35 µg/g was achieved, demonstrating the excellent potential of LIBS-LIF in the exploration of uranium in natural resources [152]. LIBS-LIF could also eliminate spectral interference effectively and improve the ability of LIBS to detect trace heavy metals (0.6 ppm Pb) in soil [153]. Utilizing the combination of carbon in steel industry and nitrogen in ambient gas to generate carbon-nitrogen (CN) radicals by LIBS resonantly, the excited CN radicals could be stimulated by laser ($\lambda_{\text{ex}} = 421.60$ nm) to emit fluorescence ($\lambda_{\text{em}} = 388.34$ nm) [154]. Remote detection of atmospheric haloalkanes of interest at a high altitude poses considerable technological or logistic challenges. Laser sources could be used to remotely excite and fragment the target haloalkane molecules, followed by their identification and quantification using optical emission [155]. Hitachi's Vulcan Handheld LIBS Metal Analyzer represents one of the fastest metal analyzers available today. Results are available in seconds with only a pull of the trigger [156]. LIBS can be used to determine the elemental composition of bacterial cells; the use of standoff or remote apparatus helps minimize the risk to the operators during bacteriological identification of unknown specimens [157].

11. Detection of Viruses in Wastewater Using LIF

One of the most important aspects in controlling a viral outbreak is monitoring the number of infected people in a population. However, with the possibility of a large population not tested for the virus in question, they will not be included in the number of infected cases, leading to an inaccurate estimate of infection cases. One such method is to screen wastewater for viruses and use the viral count as a metric for the number of infected [158]. This method allows outbreaks to be predicted weeks in advance without delays in getting the total population tested.

There are several methods that can be used to detect these viruses, but most employ either labelling of viral particles or using polymerase chain reaction amplification of the viral DNA or RNA [159]. Those which utilize labels, primarily use immunolabeling with fluorescent labels that can be detected through LIF [160]. This technology has been demonstrated to be invaluable during the COVID 19 pandemic as these data allowed for governments to limit citizen virus exposure by issuing lockdowns before they became obviously necessary based on case data [161].

12. Fluorescence Detection of Transition Metal Oxide Nanoparticles

Metal oxide nanoparticles (MONPs)— Al_2O_3 , CeO_2 , CuO , Fe_3O_4 , Mn_3O_4 , TiO_2 , ZnO , ZrO_2 —represent a field of materials chemistry that has attracted considerable interest in the last couple of decades due to their industrial and technological applications [162]. MONPs are employed as biomedical materials in biosensing, dentistry, diagnosis, immunotherapy, regenerative medicine, tissue therapy, and wound healing. Their surface properties can be tailor-made by introducing ligand functionality that provides target specificity, for example, the addition of antibodies to their surfaces with specificity for a target cell [163]. Advances in the development of functionalized MONPs are witnessed over a broad range of applications including biomedical imaging, cancer treatment, catalysis, chemical sensing, drug delivery, theranostics, and treatment of wastewater containing heavy metals [164,165]. In addition, nanoparticles can effectively be combined with antibiotic drugs because it is easier for the nanoparticles to enter bacterial cells compared with antibiotic drugs alone, as nanoparticles are endocytosed and can be functionalized to target specific cells, whereas the drugs alone passively diffuse into cells [166]. Supposedly, nanoparticles are able to participate in subcellular reactions because their size is similar to biological molecules. For instance, ZnO nanoparticles have been found to inhibit *Staphylococcus aureus* (Gram-positive bacteria) cells. It is well-known that they have ability to penetrate the *Pseudomonas aeruginosa* (Gram-negative bacteria) and *S. aureus* (Gram-positive bacteria) cells [167]. As most cell membranes are negatively charged, it is postulated that positively charged nanoparticles have a higher affinity for bacteria. However, their antifungal, antimicrobial and antiviral properties come along with biotoxicology [167]. Exposure to Al_2O_3 nanoparticles may result in adverse health consequences of disturbed redox homeostasis, hepatocellular toxicity, neurodegeneration, and DNA damage [168]. Furthermore, PbO nanoparticles are graded as toxic and dangerous for the environment and human health [169]. The greater surface area per mass of MONPs renders these nanoparticles biologically more active [170]. Public health concerns about their unintended release in the environment are triggering the need for a better understanding of their potential hazards to humans, and it is imperative to assess their eco-toxicological impact on aquatic eco-systems. MONPs are reported to have wide-ranging antimicrobial activities and be potent against bacteria, viruses, and protozoans. Normally, smaller nanoparticles have higher antibacterial activity and are more toxic (than big nanoparticles) because their larger surface area-to-volume ratio enhanced production of reactive oxygen species. These oxygen species can be produced by nanoparticles through a variety of mechanisms including surface-catalyzed photodecomposition of O_2 , Fenton-like reactions, and reactions with organic molecules on the nanoparticle surfaces [171]. Exposed surfaces that are less stable require less energy to form oxygen-free functions, thus increasing the antimicrobial activity of the nanoparticles [172].

A predominant mechanism leading to toxicity involves damage to proteins, cell membranes and DNA [173]. Benchmark dose analysis is an effective tool to rank sensitivity and toxicity across MONPs. Specifically, bronchial (BEAS-2B) and alveolar epithelial cells (A549) are exposed to a concentration range (0.4–100 $\mu\text{g}/\text{mL}$) of aqueous MONP suspension. Eight toxicity endpoints representing the integrity of lysosomal/cell membrane, oxidative stress level, glutathione based detoxification (glutathione S-transferase), oxidative metabolism (cytochrome P450), alteration of the mitochondrial membrane potential, alteration of phase II antioxidative enzyme (NAD(P)H:quinone oxidoreductase), and de novo DNA synthesis can be determined. The sensitivity/toxicity decreases in the following order: $\text{ZnO} > \text{CuO} > \text{TiO}_2 > \text{ZrO}_2 > \text{CeO}_2$ when lung bronchial cells are exposed to these nanoparticles [174]. Algorithmic examination of MONPs by categorization into toxicologically distinct clusters has divided them into sub-classes based on their dose-response-recovery similarity. Fe_2O_3 , SiO_2 and TiO_2 nanoparticles showed signs of elevated immune system activity and cell membrane damage; ZnO and CeO_2 nanoparticles exhibited comparatively reduced toxicity across all five responses [175]. The potential toxic effect of superparamagnetic iron oxide nanoparticles on various cell lines has centered on cellular and molecular mechanisms in animal models [176]. A high dose of biologically and chemically synthesized CuO nanoparticles induced adverse effects on hepatic, renal and splenic tissues. At the same dose level, the biologically synthesized CuO nanoparticles evoked more potent toxic effects than the chemically synthesized ones [177]. Particularly, it has been confirmed that MONPs may induce serious genotoxic effects on various biological targets. Given the difficulties of experimental assays for estimating the genotoxicity of MONPs on diverse biological targets, development of alternative methodologies is crucial to establish their level of safety. In silico modelling approaches, such as quantitative structure–toxicity relationships based on perturbation theory machine learning, are now considered a promising solution for predicting their genotoxicity rapidly and cost-efficiently [178]. When a model of luminescent bacteria, *Vibrio fischeri*, was employed to test the acute toxicity, the median effective concentration were 12 mg L^{-1} for ZnO nanoparticles and 119 mg L^{-1} for CuO nanoparticles. For binary nanoparticle mixtures, the combined effect was synergistic revealing a complex pattern of interactions [179].

Various antitoxic strategies, involving coatings and surface treatments, are emerging to decrease the harmful results while maintaining the favorable properties of MONPs [180]. Mohanan et al. recommends adopting surface functionalization strategies for reducing toxic response of ZnO nanoparticles in various applications [181]. Different strategies of surface modification and functionalization of colloidal ZnO nanoparticles have been reported to lower their toxicity [182]. However, their surface chemistry is not as established as that of silica and alumina and modification of ZnO nanoparticle surface area could lead to release of Zn^{2+} ions that enhance ROS production. Fe_2O_3 nanoparticles can be coated with tartaric/adipic acid with potential for use as oral iron supplements [183]. Different coatings (dextran, chitosan, polyethylene glycol, carboxy-silane, and silica) can affect the toxicity elicited by super-paramagnetic iron oxide nanoparticles in developing zebrafish (*Danio rerio*). Ranging from embryotoxicity parameters (survival, hatching rate, and anatomical malformations) to behavioral patterns (locomotion during the exploration of a new environment, thigmotaxis, and the escape response to an aversive stimulus), the toxic effect depends on the physical size, hydrodynamic diameters, and zeta potential of the coated nanoparticles [184]. Mn_3O_4 nanoparticles can be doped with Zn, Cu or Cr to regulate the Fermi energy level far away from the valence band energy, thus generating a lower amount of $\bullet\text{OH}$ and hence reducing the toxicity [185].

In addition to toxicity [186], MONPs can impose rather unexpected but quite significant effects on the structure and activity of biochemicals adsorbed on their surfaces. Understanding of the interaction of nanoparticles with biomolecules (such as ZnO with cysteine thiol groups in proteins) [187,188] is very important, as it can help better design nanocomposites for applications in diagnostics, drug delivery, cell monitoring, and sensors. It is well documented that protein adsorption is the first process that occurs upon implanta-

tion of a biomaterial into the physiological environment. Hence, human cells do not contact the biomaterial directly, but interact with the adsorbed protein layer. The orientation, conformation and packing arrangement of proteins are controlled by their tertiary structures in relation to active sites at the nanoparticle surface. For instance, the decrease in fluorescence intensity caused by collisional quenching, as revealed by the Stern–Volmer plots, indicated an effective static quenching process by TiO₂ nanoparticles whereas SnO₂ nanoparticles had a lower quenching efficiency for bovine serum albumin fluorescence [189]. CeO₂ nanoparticles triggered the transition of hen egg white lysozyme secondary structure from α -helix to β -sheet and induced the hydrophobic region of lysozyme to become exposed to the solvent [190]. They also interact with bovine serum albumin with minor conformational changes in the biomolecular structure [191]. MONPs all interacted with the phosphate backbone of DNA, but exhibited different DNA adsorption affinity [192,193]. Some adsorbed DNA without quenching the fluorescence, while others strongly quenched adsorbed fluorophores. They also displayed different affinity toward anions as probed by desorption of DNA as a signaling molecule [194].

Surface modification with organic dyes, molecular fluorophores, and fluorescent labels/probes made MONPs one of the most useful tools that chemistry has provided to biomedical research, enabling the intracellular monitoring of targeted species by fluorescence lifetime imaging microscopy for various medical and biological purposes [195]. It allows for upconversion to theranostics that unite diagnostic and therapeutic applications to form a single agent, allowing for diagnosis, drug delivery and treatment response monitoring [196]. Using the fluorescence lifetime difference exhibited by native doxorubicin (~1 ns) compared to conjugated doxorubicin (~4.6 ns), the intracellular release of conjugated doxorubicin was in situ monitored in H1299 lung cancer cells with time [197]. Environmental sensitivity of the fluorescence lifetime offers insights into the local environment of a nanoparticle or its interaction with surrounding biomolecules [198]. Titania (TiO₂) and zirconia (ZrO₂) serve as useful models for metal-oxide nanoparticles due to their identical stoichiometry, comparable acid/base behavior (surface hydroxyl groups' point of zero zeta potential = 5.8 and 6.7) and similar refractive indices (2.5 and 2.2, compared with 1.7 for alumina Al₂O₃). Fluorescent magnetic Eu³⁺-doped gadolinium oxide (Gd₂O₃) nanoparticles were successfully fabricated for biomedical applications [199]. Luminescent behaviors were different between the pristine and modified europium-doped lutetium-oxide (Eu:Lu₂O₃) nanoparticles due to the influence of surface ligands or silver (Ag) on their emission properties [200]. The fluorescence lifetime (τ) is expressed as $\tau_0 = 1/(\Gamma + \Gamma_m + k_{nr})$ where Γ is radiative decay, k_{nr} is the non-radiative decay rate and subscript m denotes metal, while the quantum efficiency of a scintillator material in the presence of a nearby metal Q_0 is expressed as $Q_0 = (\Gamma + \Gamma_m)/(\Gamma + \Gamma_M + k_{nr})$ and it indicates the possibility to simultaneously decrease the decay time by 14% and increase the luminescence intensity by introducing Γ_m . Attachment of GFP molecules to TiO₂ and cadmium oxide (CdO) was investigated with time correlated single photon counting [201]. Time-resolved experiments show that the τ of GFP molecules bound to MONPs got shortened by 43% and 22% for TiO₂ and CdO, respectively, due to photoinduced electron transfer caused by the interaction of GFP molecules (donor) and MONPs (acceptor). Addition of polystyrene nanoparticles ($n = 1.59$) to an aqueous solution of the common fluorescence dye molecule, Alexa 430, with a low quantum yield, led to a significant enhancement in quantum yield and an associated increase of the fluorescent lifetime by up to 55% [202]. The increased quantum yield could be attributed to the hydrophobic effect on the structure of water ($n = 1.33$) in the boundary layer around the polystyrene particles in suspension. Research into organic dye-sensitized solar cells was reinvigorated by the improvement of organic dye sensitizers designed to have electron donor and electron acceptor motifs located at opposite ends of the molecule that were connected through a π -bridge motif. Certain organic dyes were found to prevent injected electrons within the titania conduction band from being intercepted by the oxidized redox species [203]. Structurally, the D35 dye contains a triphenylamine donor motif, a thiophene π -bridge, and a cyanoacrylic acid acceptor motif [203]. When the

D35 dye is bound to the titania nanoparticle surface at full coverage, the butoxyl groups form a steric barrier at the electrode/electrolyte interface, inhibiting recombination. The butoxyl groups also prevent dye molecules from aggregating to result in shorter excited state lifetimes.

There has been an increase in the use of MONPs in the fluorescent detection of other molecules, which in many cases can be altered and used as a means of detecting the nanoparticles themselves [204]. For instance, Venkatesan et al. [205] attempted to use ZnO nanoparticles as a means of detecting picric acid and found that their fluorescence increased dramatically. Thus, by extension, picric acid can be used to detect ZnO nanoparticles [205]. Similarly, by attaching a silane linker and the fluorescent dye to TiO₂ nanoparticles for cell imaging, Kokot et al. [206] found this strategy to be applicable to detection of the nanoparticles in water samples. Finally, Zhou et al. [207,208] used fluorescently labelled DNA aptamers for the detection of specific species (e.g., Ochratoxin A and Aflatoxin B) in food samples. In their work, the aptamers were not chemically bonded to nanoparticles, making them easily detached in the presence of the target species as the three dimensional shape assumed by the aptamers allowed them to overcome their adsorption onto the nanoparticles, resulting in a lower fluorescence quenching effect for the development of a sensitive detection method. Our laboratory has developed a similar detection method for TiO₂ nanoparticles involving coating with fluorescein isothiocyanate (FITC) labelled anti-dopamine DNA aptamers, as illustrated in Figure 3. In this method, fluorescently labeled aptamers are adsorbed onto nanoparticles, unbound aptamers are removed, and bound aptamers are removed by adding their target, separated, and detected by LIF in order to determine the concentration of nanoparticles in the sample.

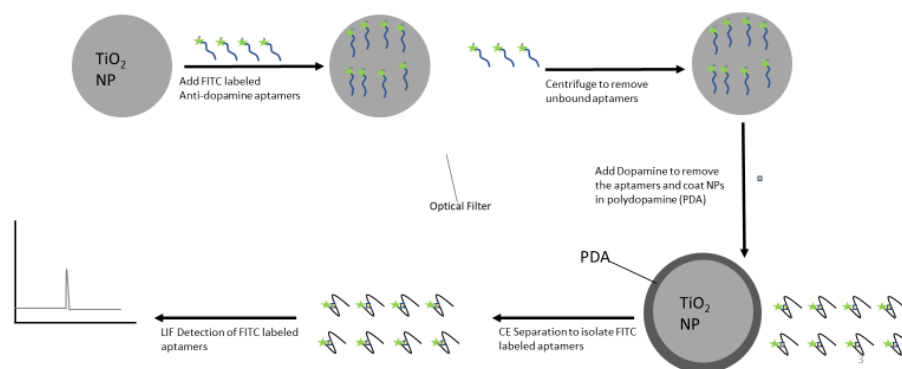


Figure 3. Detection method for titania nanoparticles (TiO₂ NPs) based on dopamine aptamer.

13. Conclusion/Future Developments

LIF technology, despite being developed during the latter half of the 20th century, has only grown in usefulness as technology has developed. The advances in laser, detector, fiber optics, and fluorescent labeling technologies have transformed a technique that was once difficult to use, and limited in its scope, into one of the most prominent detection and imaging techniques. In addition, as the fields of biology and biochemistry have advanced, the needs for fluorescence detection has dramatically increased, further increasing demand for LIF. Moreover, the use of nanoparticles in these fields have provided methods of detecting nanoparticles by LIF, something which will become more necessary as MONPs are found in increasing quantities in the environment [209]. With advances in new technologies such as 3D printing, there is a promising future for LIF instrumentation design and manufacturing [210].

Author Contributions: Writing—original draft preparation A.T.T. and E.P.C.L.; writing—review and editing, A.T.T. and E.P.C.L.; visualization, A.T.T.; supervision E.P.C.L.; project administration, E.P.C.L.; funding acquisition, E.P.C.L. All authors have read and agreed to the published version of the manuscript.

Funding: Financial support was received from Natural Sciences and Engineering Research Council of Canada (NSERC) through grant number RGPIN-2018-05320.

Institutional Review Board Statement: Not applicable.

Informed Consent Statement: Not applicable.

Data Availability Statement: Not applicable.

Conflicts of Interest: The authors declare no conflict of interest.

References

- Gerardi, A.R.; Lubbeck, J.L.; Colyer, C.L. Dimethylditetradecylammonium bromide (2C 14DAB) as a self-assembled surfactant coating for detection of protein-dye complexes by CE-LIF. *J. Solid State Electrochem.* **2009**, *13*, 633–638. [CrossRef]
- Khan, S.; Newport, D.; Le Calvé, S. Gas Detection Using Portable Deep-UV Absorption. *Sensors* **2019**, *19*, 5210. [CrossRef] [PubMed]
- Zare, R.N. My life with LIF: A personal account of developing laser-induced fluorescence. *Annu. Rev. Anal. Chem.* **2012**, *5*, 1–14. [CrossRef]
- Wang, S.; Chen, L.; Jangili, P.; Sharma, A.; Li, W.; Hou, J.T.; Qin, C.; Yoon, J.; Kim, J.S. Design and applications of fluorescent detectors for peroxynitrite. *Coord. Chem. Rev.* **2018**, *374*, 36–54. [CrossRef]
- Hofzumahaus, A.; Holland, F. Laser-induced fluorescence based detection system for measurement of tropospheric OH using 308 nm excitation at low pressure. *Opt. Methods Atmos. Chem.* **1993**, *1715*, 163–173. [CrossRef]
- Knewton, K.E.; Rane, D.; Peterson, B.R. Targeting Fluorescent Sensors to Endoplasmic Reticulum Membranes Enables Detection of Peroxynitrite during Cellular Phagocytosis. *ACS Chem. Biol.* **2018**, *13*, 2595–2602. [CrossRef]
- Gu, B.; Liu, C.; Wu, Y.; Zhang, C.; Shen, Y.; Liu, M. Application of a colorimetric and near-infrared fluorescent probe in peroxynitrite detection and imaging in living cells. *ACS Omega* **2020**, *5*, 27530–27535. [CrossRef]
- Ihara, D.; Hazama, H.; Nishimura, T.; Morita, Y.; Awazu, K. Fluorescence detection of deep intramucosal cancer excited by green light for photodynamic diagnosis using protoporphyrin IX induced by 5-aminolevulinic acid: An ex vivo study. *J. Biomed. Opt.* **2020**, *25*, 1. [CrossRef] [PubMed]
- Weber, M.; Yamada, N.; Tian, X.; Bull, S.D.; Minoshima, M.; Kikuchi, K.; Mackenzie, A.B.; James, T.D. Sensing Peroxynitrite in Different Organelles of Murine RAW264.7 Macrophages With Coumarin-Based Fluorescent Probes. *Front. Chem.* **2020**, *8*, 1–10. [CrossRef]
- Wang, K.K.; Song, M.W.K.; Norbasch, A.; Prendergas, F. What Can be Expected from Laser Induced Fluorescence? Available online: http://www.oeso.org/OESO/books/Vol_5_Eso_Junction/Articles/art299.html (accessed on 30 May 2021).
- Szarka, M.; Szigeti, M.; Guttman, A. Imaging Laser-Induced Fluorescence Detection at the Taylor Cone of Electrospray Ionization Mass Spectrometry. *Anal. Chem.* **2019**, *91*, 7738–7743. [CrossRef]
- Jin, Y.; Chen, C.; Meng, L.; Chen, J.; Li, M.; Zhu, Z.; Lin, J. A CE-LIF method to monitor autophagy by directly detecting LC3 proteins in HeLa cells. *Analyst* **2012**, *137*, 5571–5575. [CrossRef] [PubMed]
- Qiao, J.; Qi, L.; Mu, X.; Chen, Y. Monolith and coating enzymatic microreactors of l-asparaginase: Kinetics study by MCE-LIF for potential application in acute lymphoblastic leukemia (ALL) treatment. *Analyst* **2011**, *136*, 2077–2083. [CrossRef] [PubMed]
- Feás, X.; Fente, C.A.; Cepeda, A. Fast and sensitive new high performance liquid chromatography laser induced fluorescence (HPLC-LIF) method for quinine. Comparative study in soft drinks. *J. Liq. Chromatogr. Relat. Technol.* **2009**, *32*, 2600–2614. [CrossRef]
- Kang, J.; Wang, Y.; Chen, Y.; Li, R. Fast and ultrasensitive detection of toxic heavy metals in water by LIBS-LIF technique. *Opt. InfoBase Conf. Pap.* **2017**, *F83-A*, 1–3. [CrossRef]
- Bandeira, R.D.D.C.C.; Uekane, T.M.; Cunha, C.P.D.; Rodrigues, J.M.; la Cruz, M.H.C.D.; Godoy, R.L.D.O.; Fioravante, A.D.L. Comparison of High Performance Liquid Chromatography with Fluorescence Detector and with Tandem Mass Spectrometry Methods for Detection and Quantification of Ochratoxin A in Green and Roasted Coffee Beans. *Arch. Biol. Technol.* **2013**, *56*, 911–920. [CrossRef]
- Baldwin, M.A. Protein identification by mass spectrometry: Issues to be considered. *Mol. Cell. Proteomics* **2004**, *3*, 1–9. [CrossRef]
- Gabbarini, V.; Rossi, R.; Ciparisse, J.F.; Malizia, A.; Divizia, A.; De Filippis, P.; Anselmi, M.; Carestia, M.; Palombi, L.; Divizia, M.; et al. Laser-induced fluorescence (LIF) as a smart method for fast environmental virological analyses: Validation on Picornaviruses. *Sci. Rep.* **2019**, *9*, 3–9. [CrossRef]
- Sun, X. Design, Synthesis and Evaluation of Fluorescent Sensors for the Detection of Saccharide and Reactive Oxygen Species. Ph.D. Thesis, University of Bath, Bath, UK, 2015.
- Wu, L.; Sedgwick, A.C.; Sun, X.; Bull, S.D.; He, X.P.; James, T.D. Reaction-Based Fluorescent Probes for the Detection and Imaging of Reactive Oxygen, Nitrogen, and Sulfur Species. *Acc. Chem. Res.* **2019**, *52*, 2582–2597. [CrossRef]
- Laser-Induced Fluorescence. Available online: <https://clu-in.org/characterization/technologies/lif.cfm> (accessed on 30 May 2021).
- Perry, S.J. *Design of a Low-Cost Capillary Electrophoresis Laser-Induced Fluorescence System: Lessons Learned When Trying to Build the Lowest Possible Cost System*; Brigham Young University: Provo, UT, USA, 2018.

23. NASA's New Way to Track Formaldehyde. Available online: <https://www.nasa.gov/topics/technology/features/formaldehyde-track.html> (accessed on 30 August 2021).
24. Cazorla, M.; Wolfe, G.M.; Bailey, S.A.; Swanson, A.K.; Arkinson, H.L.; Hanisco, T.F. A new airborne laser-induced fluorescence instrument for in situ detection of formaldehyde throughout the troposphere and lower stratosphere. *Atmos. Meas. Tech.* **2015**, *8*, 541–552. [[CrossRef](#)]
25. Day, D.A.; Wooldridge, P.J.; Dillon, M.B.; Thornton, J.A.; Cohen, R.C. A thermal dissociation laser-induced fluorescence instrument for in situ detection NO₂, peroxy nitrates, alkyl nitrates, and HNO₃. *J. Geophys. Res. Atmos.* **2002**, *107*, ACH-4. [[CrossRef](#)]
26. Rollins, A.W.; Rickly, P.S.; Gao, R.S.; Ryerson, T.B.; Brown, S.S.; Peischl, J.; Bourgeois, I. Single-photon laser-induced fluorescence detection of nitric oxide at sub-parts-per-trillion mixing ratios. *Atmos. Meas. Tech.* **2020**, *13*, 2425–2439. [[CrossRef](#)]
27. Rogers, S.R.; Webster, T.; Livingstone, W.; O'Driscoll, N.J. Airborne Laser-Induced Fluorescence (LIF) Light Detection and Ranging (LiDAR) for the Quantification of Dissolved Organic Matter Concentration in Natural Waters. *Estuaries Coast* **2012**, *35*, 959–975. [[CrossRef](#)]
28. St. Germain, R. Laser-Induced Fluorescence Primer. Available online: <https://www.dakotatechnologies.com/info/newsletters/article/2016/03/16/laser-induced-fluorescence-primer> (accessed on 31 May 2021).
29. Caneve, L.; Colao, F.; Del Franco, M.; Palucci, A.; Pistilli, M.; Spizzichino, V. Multispectral imaging system based on laser-induced fluorescence for security applications. In Proceedings of the Optics and Photonics for Counterterrorism, Crime Fighting, and Defence XII, Edinburgh, UK, 26–27 September 2016; Volume 9995, p. 8. [[CrossRef](#)]
30. Zhange, Z.; Park, J.; Barrett, H.; Dooley, S.; Davies, C.; Verhagen, M.F. Capillary Electrophoresis-Sodium Dodecyl Sulfate with Laser-Induced Fluorescence Detection As a Highly Sensitive and Quality Control-Friendly Method for Monitoring Adeno-Associated Virus Capsid Protein Purity. *Hum. Gene Ther.* **2021**, *32*, 628–637. [[CrossRef](#)]
31. Cai, S.Z.; Zhang, Q.F.; Xu, X.P.; Hu, D.H.; Qu, Y.M. Research of Laser Induced Fluorescence Detection Techniques Based on Microfluidic Devices. *Adv. Mater. Res.* **2014**, *989–994*, 2761–2763.
32. Overview of Filters and Light Sources. Available online: [https://www.thermofisher.com/ca/en/home/life-science/cell-analysis/cell-analysis-learning-center/molecular-probes-school-of-fluorescence/fluorescence-basics/overview-filters-light-sources.html#:~:text=1\)Themostpopularsources,varyingintensityacrosst](https://www.thermofisher.com/ca/en/home/life-science/cell-analysis/cell-analysis-learning-center/molecular-probes-school-of-fluorescence/fluorescence-basics/overview-filters-light-sources.html#:~:text=1)Themostpopularsources,varyingintensityacrosst) (accessed on 28 May 2021).
33. Fulton, M.L. Color correction of metal halide arc lamp sources. *Opt. Eng.* **2003**, *42*, 2155. [[CrossRef](#)]
34. Lee, A.C.H.; Elson, D.S.; Neil, M.A.; Kumar, S.; Ling, B.W.; Bello, F.; Hanna, G.B. Solid-state semiconductors are better alternatives to arc-lamps for efficient and uniform illumination in minimal access surgery. *Surg. Endosc.* **2009**, *23*, 518–526. [[CrossRef](#)] [[PubMed](#)]
35. Jenkins, R.; Aldwell, B.; Yin, S.; Meyer, M.; Robinson, A.J.; Lupoi, R. Energy efficiency of a quartz tungsten halogen lamp: Experimental and numerical approach. *Therm. Sci. Eng. Prog.* **2019**, *13*, 100385. [[CrossRef](#)]
36. Davidson, M.W. Tungsten-Halogen Incandescent Lamps. Available online: <http://zeiss-campus.magnet.fsu.edu/articles/lightsources/tungstenhalogen.html> (accessed on 28 May 2021).
37. Burgin, R.; Edwards, E. The Tungsten Lamp Decade. *Light. Res. Technol.* **1970**, *2*, 95–108. [[CrossRef](#)]
38. Aswani, K.K. Emerging LED Technologies for Fluorescence Microscopy. *Microsc. Today* **2016**, *24*, 22–27. [[CrossRef](#)]
39. Dang, F.; Geng, X.; Li, J.; Wang, J.; Guan, Y. A miniaturized and high sensitive dual channel fluorimeter based on compact collinear optical arrangement. *Talanta* **2020**, *211*, 120698. [[CrossRef](#)] [[PubMed](#)]
40. Wood, M. How do LEDs Work? Part 3. Available online: <https://www.mikewoodconsulting.com/articles/Protocol%20Fall%202009%20-%20How%20do%20LEDs%20Work3.pdf> (accessed on 20 September 2021).
41. Sato, K.; Watanabe, R.; Hanaoka, H.; Nakajima, T.; Choyke, P.L.; Kobayashi, H. Comparative effectiveness of light emitting diodes (LEDs) and lasers in near infrared photodynamic therapy. *Oncotarget* **2016**, *7*, 14324–14335. [[CrossRef](#)]
42. Tango, W.J.; Link, J.K.; Zare, R.N. Spectroscopy of K2 Using Laser-Induced Fluorescence. *J. Chem. Phys.* **1968**, *49*, 4264–4268. [[CrossRef](#)]
43. Da Silva, J.M.; Utkin, A.B. Application of laser-induced fluorescence in functional studies of photosynthetic biofilms. *Processes* **2018**, *6*, 227. [[CrossRef](#)]
44. Wang, G.; Lou, Y.; Wang, R.; Yan, D.; Li, X.; Zhao, X.; Chen, D.; Zhao, Q. Design of remote laser-induced fluorescence system's acquisition circuit. In Proceedings of the AOPC 2017: Optical Spectroscopy and Imaging, Beijing, China, 4–6 June 2017; Volume 10461, p. 34. [[CrossRef](#)]
45. Li, H.; Van't Hag, L.; Yousef, Y.A.; Melø, T.B.; Razi Naqvi, K. Single shot laser flash photolysis with a fibre-coupled reference beam monitor. *Photochem. Photobiol. Sci.* **2013**, *12*, 404–406. [[CrossRef](#)] [[PubMed](#)]
46. Boutonnet, A.; Morin, A.; Petit, P.; Vicendo, P.; Poinsot, V.; Couderc, F. Pulsed lasers versus continuous light sources in capillary electrophoresis and fluorescence detection studies: Photodegradation pathways and models. *Anal. Chim. Acta* **2016**, *912*, 146–155. [[CrossRef](#)] [[PubMed](#)]
47. Snyder, J.A.; Amori, A.R.; Odoi, M.Y.; Stern, H.A.; Peterson, J.J.; Krauss, T.D. The influence of continuous vs. pulsed laser excitation on single quantum dot photophysics. *Phys. Chem. Chem. Phys.* **2014**, *16*, 25723–25728. [[CrossRef](#)] [[PubMed](#)]
48. Smith, H.D.; McKay, C.P.; Duncan, A.G.; Sims, R.C.; Anderson, A.J.; Grossl, P.R. An instrument design for non-contact detection of biomolecules and minerals on Mars using fluorescence. *J. Biol. Eng.* **2014**, *8*, 1–14. [[CrossRef](#)] [[PubMed](#)]
49. Fellner, L.; Kraus, M.; Gebert, F.; Walter, A.; Duschek, F. Multispectral LIF-based standoff detection system for the classification of cbe hazards by spectral and temporal features. *Sensors* **2020**, *20*, 2524. [[CrossRef](#)]

50. Babichenko, S.; Gala, J.L.; Bentahir, M.; Piette, A.S.; Poryvkina, L.; Rebane, O.; Smits, B.; Sobolev, I.; Soboleva, N. Non-Contact, Real-Time Laser-Induced Fluorescence Detection and Monitoring of Microbial Contaminants on Solid Surfaces Before, During and After Decontamination. *J. Biosens. Bioelectron.* **2018**, *9*, 255. [CrossRef]
51. Gratton, E.; Barry, N.P.; Beretta, S.; Celli, A. Multiphoton fluorescence microscopy. *Methods* **2001**, *25*, 103–110. [CrossRef]
52. Miller, D.R.; Jarrett, J.W.; Hassan, A.M.; Dunn, A.K. Deep tissue imaging with multiphoton fluorescence microscopy. *Curr. Opin. Biomed. Eng.* **2017**, *4*, 32–39. [CrossRef]
53. Ash, C.; Dubec, M.; Donne, K.; Bashford, T. Effect of wavelength and beam width on penetration in light-tissue interaction using computational methods. *Lasers Med. Sci.* **2017**, *32*, 1909–1918. [CrossRef]
54. Xu, C.; Zipfel, W.; Shear, J.B.; Williams, R.M.; Webb, W.W. Multiphoton fluorescence excitation: New spectral windows for biological nonlinear microscopy. *Proc. Natl. Acad. Sci. USA* **1996**, *93*, 10763–10768. [CrossRef] [PubMed]
55. Zhang, J.; Campbell, R.E.; Ting, A.Y.; Tsien, R.Y. Creating new fluorescent probes for cell biology. *Nat. Rev. Mol. Cell Biol.* **2002**, *3*, 906–918. [CrossRef] [PubMed]
56. CF@DYES Next Generation Fluorescent Dyes. Available online: <https://biotium.com/technology/cf-dyes/> (accessed on 30 May 2021).
57. Tsien, R.Y. The green fluorescent protein. *Annu. Rev. Biochem.* **1998**, *67*, 509–544. [CrossRef] [PubMed]
58. Remington, S.J. Green fluorescent protein: A perspective. *Protein Sci.* **2011**, *20*, 1509–1519. [CrossRef]
59. Guo, P.; Wang, Y.; Zhuang, Q. Highly sensitive and selective biosensor for heparin detection with rhodamine B-labelled peptides as fluorescent bioreceptors. *Sens. Actuators B Chem.* **2019**, *299*, 126873. [CrossRef]
60. Wichgers Schreur, P.J.; Kortekaas, J. Single-Molecule FISH Reveals Non-selective Packaging of Rift Valley Fever Virus Genome Segments. *PLoS Pathog.* **2016**, *12*, 1–21. [CrossRef]
61. Berneschi, S.; Baldini, F.; Applicata, F.; Carrara, N.; Cosci, A.; Enrico, R.; Cosi, F.; Applicata, F.; Carrara, N.; Farnesi, D.; et al. Localized immunoassay in flow-through optical microbubble resonator (conference presentation). In Proceedings of the Silicon Photonics and Photonic Integrated Circuits V, Brussels, Belgium, 3–7 April 2016; Volume 9891, p. 2227812. [CrossRef]
62. Ferrara, F.; Listwan, P.; Waldo, G.S.; Bradbury, A.R.M. Fluorescent labeling of antibody fragments using split GFP. *PLoS ONE* **2011**, *6*, 1–9. [CrossRef]
63. McConnell, E.M.; Ventura, K.; Dwyer, Z.; Hunt, V.; Koudrina, A.; Holahan, M.R.; Derosa, M.C. In Vivo Use of a Multi-DNA Aptamer-Based Payload/Targeting System to Study Dopamine Dysregulation in the Central Nervous System. *ACS Chem. Neurosci.* **2019**, *10*, 371–383. [CrossRef]
64. Chen, Q.; Zhao, W.; Fung, Y. Determination of acrylamide in potato crisps by capillary electrophoresis with quantum dot-mediated LIF detection. *Electrophoresis* **2011**, *32*, 1252–1257. [CrossRef]
65. Hsu, S.C.; Chen, Y.H.; Tu, Z.Y.; Han, H.V.; Lin, S.L.; Chen, T.M.; Kuo, H.C.; Lin, C.C. Highly Stable and Efficient Hybrid Quantum Dot Light-Emitting Diodes. *IEEE Photonics J.* **2015**, *7*, 1–10. [CrossRef]
66. Borah, P.; Siboh, D.; Kalita, P.K.; Sarma, J.K.; Nath, N.M. Quantum confinement induced shift in energy band edges and band gap of a spherical quantum dot. *Phys. B Condens. Matter* **2018**, *530*, 208–214. [CrossRef]
67. Tanaka, T. A quantum dot model for nanoparticles in polymer nanocomposites. *IEEE Trans. Dielectr. Electr. Insul.* **2019**, *26*, 276–283. [CrossRef]
68. Bai, X.F.; Zhao, Y.W.; Xin, W.; Yin, H.W. Eerdunchaolu Transition Probability and Frequency of an Electron in an Asymmetric Gaussian Confinement Potential Quantum Dot with Electromagnetic Field. *Iran. J. Sci. Technol. Trans. A Sci.* **2019**, *43*, 2027–2034. [CrossRef]
69. Ranjbar-Navazi, Z.; Omid, Y.; Eskandani, M.; Davaran, S. Cadmium-free quantum dot-based theranostics. *TrAC Trends Anal. Chem.* **2019**, *118*, 386–400. [CrossRef]
70. Gidwani, B.; Sahu, V.; Shukla, S.S.; Pandey, R.; Joshi, V.; Jain, V.K.; Vyas, A. Quantum dots: Prospectives, toxicity, advances and applications. *J. Drug Deliv. Sci. Technol.* **2021**, *61*, 102308. [CrossRef]
71. Ca, N.X.; Hien, N.T.; Luyen, N.T.; Lien, V.T.K.; Thanh, L.D.; Do, P.V.; Bau, N.Q.; Pham, T.T. Photoluminescence properties of CdTe/CdTeSe/CdSe core/alloyed/shell type-II quantum dots. *J. Alloys Compd.* **2019**, *787*, 823–830. [CrossRef]
72. Rana, M.; Jain, A.; Rani, V.; Chowdhury, P. Glutathione capped core/shell CdSeS/ZnS quantum dots as a medical imaging tool for cancer cells. *Inorg. Chem. Commun.* **2020**, *112*, 107723. [CrossRef]
73. Peng, X.; Schlamp, M.C.; Kadavanich, A.V.; Alivisatos, A.P. Epitaxial growth of highly luminescent CdSe/CdS core/shell nanocrystals with photostability and electronic accessibility. *J. Am. Chem. Soc.* **1997**, *119*, 7019–7029. [CrossRef]
74. Smith, A.M.; Mohs, A.M.; Nie, S. Tuning the optical and electronic properties of colloidal nanocrystals by lattice strain. *Nat. Nanotechnol.* **2009**, *4*, 56–63. [CrossRef] [PubMed]
75. Adegoke, O.; Seo, M.W.; Kato, T.; Kawahito, S.; Park, E.Y. An ultrasensitive SiO₂-encapsulated alloyed CdZnSeS quantum dot-molecular beacon nanobiosensor for norovirus. *Biosens. Bioelectron.* **2016**, *86*, 135–142. [CrossRef]
76. Bailey, R.E.; Nie, S. Alloyed semiconductor quantum dots: Tuning the optical properties without changing the particle size. *J. Am. Chem. Soc.* **2003**, *125*, 7100–7106. [CrossRef] [PubMed]
77. AbouElhamd, A.R.; Al-Sallal, K.A.; Hassan, A. Review of core/shell quantum dots technology integrated into building's glazing. *Energies* **2019**, *12*, 1058. [CrossRef]
78. Oh, E.; Liu, R.; Nel, A.; Gemill, K.B.; Bilal, M.; Cohen, Y.; Medintz, I.L. Meta-analysis of cellular toxicity for cadmium-containing quantum dots. *Nat. Nanotechnol.* **2016**, *11*, 479–486. [CrossRef] [PubMed]

79. Xu, G.; Zeng, S.; Zhang, B.; Swihart, M.T.; Yong, K.T.; Prasad, P.N. New Generation Cadmium-Free Quantum Dots for Biophotonics and Nanomedicine. *Chem. Rev.* **2016**, *116*, 12234–12327. [CrossRef]
80. Yaghini, E.; Turner, H.; Pilling, A.; Naasani, I.; MacRobert, A.J. In vivo biodistribution and toxicology studies of cadmium-free indium-based quantum dot nanoparticles in a rat model. *Nanomed. Nanotechnol. Biol. Med.* **2018**, *14*, 2644–2655. [CrossRef]
81. Bardhan, R.; Grady, N.K.; Cole, J.R.; Joshi, A.; Halas, N.J. Fluorescence enhancement by Au nanostructures: Nanoshells and nanorods. *ACS Nano* **2009**, *3*, 744–752. [CrossRef]
82. Joyce, C.; Fothergill, S.M.; Xie, F. Recent advances in gold-based metal enhanced fluorescence platforms for diagnosis and imaging in the near-infrared. *Mater. Today Adv.* **2020**, *7*, 100073. [CrossRef]
83. Bavali, A.; Parvin, P.; Mortazavi, S.Z.; Nourazar, S.S. Laser induced fluorescence spectroscopy of various carbon nanostructures (GO, G and nanodiamond) in Rd6G solution. *Biomed. Opt. Express* **2015**, *6*, 1679. [CrossRef]
84. Wu, T.C.; Zhao, G.; Lu, H.; Dutta, M.; Stroschio, M.A. Quantum-dot-based aptamer beacons for K⁺ detection. *IEEE Sens. J.* **2013**, *13*, 1549–1553. [CrossRef]
85. Santana, C.P.; Mansur, A.A.P.; Carvalho, S.M.; da Silva-Cunha, A.; Mansur, H.S. Bi-functional quantum dot-polysaccharide-antibody immunoconjugates for bioimaging and killing brain cancer cells in vitro. *Mater. Lett.* **2019**, *252*, 333–337. [CrossRef]
86. Dobhal, G.; Ayupova, D.; Laufersky, G.; Ayed, Z.; Nann, T.; Goreham, R.V. Cadmium-free quantum dots as fluorescent labels for exosomes. *Sensors* **2018**, *18*, 3308. [CrossRef]
87. Nagaraj, S.; Karnes, H.T. Comparison of orthogonal and collinear geometric approaches for design of a laboratory constructed diode laser induced fluorescence detector for capillary electrophoresis. *Instrum. Sci. Technol.* **2000**, *28*, 119–129. [CrossRef]
88. Fluorescence Detector FP-4020/4025. Available online: <http://www.jasco.nl/fluorescence-detector/> (accessed on 28 May 2021).
89. Dada, O.O. Laser-induced fluorescence detector with a fiber-coupled micro GRIN lens for capillary electrophoresis. *Appl. Opt.* **2020**, *59*, 4849. [CrossRef] [PubMed]
90. Fu, J.L.; Fang, Q.; Zhang, T.; Jin, X.H.; Fang, Z.L. Laser-induced fluorescence detection system for microfluidic chips based on an orthogonal optical arrangement. *Anal. Chem.* **2006**, *78*, 3827–3834. [CrossRef]
91. Lo, L.D. Integrated Laser-Induced Fluorescence Detection for Parallelizable Microfluidic Single Cell Analysis. Ph.D. Thesis, University of Toronto, Toronto, ON, Canada, 2017.
92. Pan, J.Z.; Fang, P.; Fang, X.X.; Hu, T.T.; Fang, J.; Fang, Q. A low-cost palmtop high-speed capillary electrophoresis bioanalyzer with laser induced fluorescence detection. *Sci. Rep.* **2018**, *8*, 1791. [CrossRef] [PubMed]
93. Zhao, S.; Lei, J.; Huo, D.; Hou, C.; Yang, P.; Huang, J.; Luo, X. A laser-induced fluorescent detector for pesticide residue detection based on the spectral recognition method. *Anal. Methods* **2018**, *10*, 5507–5515. [CrossRef]
94. Zhao, Y.; Li, Q.; Hu, X.M.; Yang, D.F. An LED-induced fluorescence detection system with integrated on-chip lens based on microfluidic chips technology. *Photonics Lasers Med.* **2013**, *2*, 51–57. [CrossRef]
95. Dolan, J.W. How Does It Work? Part V: Fluorescence Detectors. Available online: <http://www.lcresources.com/tsbible/34092016.pdf> (accessed on 20 September 2021).
96. Duca, Z.A.; Speller, N.C.; Cantrell, T.; Stockton, A.M. A modular, easy-to-use microcapillary electrophoresis system with laser-induced fluorescence for quantitative compositional analysis of trace organic molecules. *Rev. Sci. Instrum.* **2020**, *91*, 104101. [CrossRef]
97. Tyndall, D.; Rae, B.R.; Li, D.D.U.; Arlt, J.; Johnston, A.; Richardson, J.A.; Henderson, R.K. A high-throughput time-resolved mini-silicon photomultiplier with embedded fluorescence lifetime estimation in 0.13 μm CMOS. *IEEE Trans. Biomed. Circuits Syst.* **2012**, *6*, 562–570. [CrossRef]
98. Dorosz, P.; Baszczyk, M.; Kucewicz, W. The study of single cells in a system based on silicon photomultipliers. In Proceedings of the 2018 IEEE Nuclear Science Symposium and Medical Imaging Conference Proceedings (NSS/MIC), Sydney, NSW, Australia, 10–17 November 2018; pp. 1–2. [CrossRef]
99. Sun, X.; Krainak, M.A.; Hasselbrack, W.E.; La Rue, R.A.; Sykora, D.F. Single-photon counting at 950–1300 nm: Using InGaAsP photocathode-GaAs avalanche diode hybrid photomultiplier tubes. *J. Mod. Opt.* **2009**, *56*, 284–295. [CrossRef]
100. Concepts in Digital Imaging: Technology Photomultiplier Tubes. Available online: <http://hamamatsu.magnet.fsu.edu/articles/photomultipliers.html> (accessed on 2 June 2021).
101. Lubsandorzhev, B.K. On the history of photomultiplier tube invention. *Nucl. Instrum. Methods Phys. Res. Sect. A Accel. Spectrometers Detect. Assoc. Equip.* **2006**, *567*, 236–238. [CrossRef]
102. Saveliev, V. The recent development and study of silicon photomultiplier. *Nucl. Instrum. Methods Phys. Res. Sect. A Accel. Spectrometers Detect. Assoc. Equip.* **2004**, *535*, 528–532. [CrossRef]
103. The Inventor of the Semiconductor Laser, Super Luminosity LED and Optical Fiber Advocates Effective Energy Usage. Available online: <https://books.google.com.hk/books?id=5MRsECGrRXMC&pg=PA7&lpg=PA7&dq=The+inventor+of+the+semiconductor+laser,+super+luminosity+LED+and+optical+fiber+advocates+effective+energy+usage&source=bl&ots=NoonPzXYAp&sig=ACfU3U0aGOadPLJXxZ0GLuuf-Q7Q8TZWpA&hl=zh-CN&sa=X&ved=2ahUKewjxd3Eip7zAhWULqYKHXSEDZ0Q6AF6BAGCEAM#v=onepage&q=The%20inventor%20of%20the%20semiconductor%20laser%20C%20super%20luminosity%20LED%20and%20optical%20fiber%20advocates%20effective%20energy%20usage&f=false> (accessed on 20 September 2021).

104. Lawrence, W.G.; Varadi, G.; Entine, G.; Podniesinski, E.; Wallace, P.K. A comparison of avalanche photodiode and photomultiplier tube detectors for flow cytometry. In Proceedings of the Imaging, Manipulation, and Analysis of Biomolecules, Cells, and Tissues VI, San Jose, CA, USA, 19–24 January 2008; Volume 6859, p. 68590M. [CrossRef]
105. Avalanche Photodiodes. Available online: [https://www.rp-photonics.com/avalanche_photodiodes.html#:~:text=Typicalapplicationsofavalanchephotodiodes,timedomainreflectometers\(OTDR\)](https://www.rp-photonics.com/avalanche_photodiodes.html#:~:text=Typicalapplicationsofavalanchephotodiodes,timedomainreflectometers(OTDR)) (accessed on 3 June 2021).
106. Golovin, V.; Saveliev, V. Novel type of avalanche photodetector with Geiger mode operation. *Nucl. Instrum. Methods Phys. Res. Sect. A Accel. Spectrometers Detect. Assoc. Equip.* **2004**, *518*, 560–564. [CrossRef]
107. Ruch, M.L.; Sivels, C.B.; Czyz, S.A.; Flaska, M.; Pozzi, S.A. Comparison between silicon photomultipliers and photomultiplier tubes for pulse shape discrimination with stilbene. In Proceedings of the 2014 IEEE Nuclear Science Symposium and Medical Imaging Conference (NSS/MIC), Seattle, WA, USA, 8–15 November 2014; pp. 6–8. [CrossRef]
108. Piatek, S. What is an SiPM and How Does It Work? Available online: <https://hub.hamamatsu.com/jp/en/technical-note/how-sipm-works/index.html#:~:text=ASiPMmostresembles,a,andsmallerinsize> (accessed on 2 June 2021).
109. Yang, X.; Yan, W.; Bai, H.; Lv, H.; Liu, Z. A scanning laser induced fluorescence detection system for capillary electrophoresis microchip based on optical fiber. *Optik* **2012**, *123*, 2126–2130. [CrossRef]
110. Product Overview. Available online: <https://ibsen.com/products/> (accessed on 30 May 2021).
111. *Silicon Avalanche Photodiodes C30902 Series High Speed APDs for Analytical and Biomedical Lowest Light Detection Applications*; Perkin Elmer: Waltham, MA, USA.
112. Wu, Q.; Wang, L.; Zu, L. A LabVIEW-Based Virtual Instrument System for Laser-Induced Fluorescence Spectroscopy. *J. Autom. Methods Manag. Chem.* **2011**, *2011*, 1–7. [CrossRef]
113. What is Laser Induced Fluorescence? Available online: <https://www.edinst.com/blog/what-is-laser-induced-fluorescence/> (accessed on 14 June 2021).
114. Larson, A.P.; Ahlberg, H.; Folestad, S. Semiconductor laser-induced fluorescence detection in picoliter volume flow cells. *Appl. Opt.* **1993**, *32*, 794. [CrossRef]
115. Coulter, B. PA 800 Plus Pharmaceutical Analysis System. 2009; pp. 1–170. Available online: <https://sciex.com/products/capillary-electrophoresis/pa-800-plus-pharmaceutical-analysis-system> (accessed on 30 May 2021).
116. Applications of Planar Laser Induced Fluorescence. Available online: <https://andor.oxinst.com/learning/view/article/applications-of-planar-laser-induced-fluorescence#:~:text=PlanarLaser-InducedFluorescence%2Cor,capturedonadigitalcamera> (accessed on 19 September 2021).
117. Measurement Principles of Planar-LIF. Available online: <https://www.dantecdynamics.com/solutions-applications/solutions/fluid-mechanics/laser-induced-fluorescence/measurement-principles-of-planar-lif/> (accessed on 27 June 2021).
118. Zetalif Laser. Available online: <https://www.adelis-tech.com/product/zetalif-laser/> (accessed on 31 May 2021).
119. Capillary Electrophoresis with Laser Induced Fluorescence Detection (LIF). Available online: <https://www.agilent.com/en/products/capillary-electrophoresis-ce-ms/ce-ce-ms-systems/7100-ce-system/ce-lif> (accessed on 31 May 2021).
120. Schröder, D.; Schröder, M.; Werner, E.; Meusel, J.; Lorenzen, D.; Hennig, P. Improved laser diode for high power and high temperature applications. In Proceedings of the High-Power Diode Laser Technology and Applications VII, San Jose, CA, USA, 24–29 January 2009; Volume 7198. [CrossRef]
121. A History of the Laser: 1960–2019. Available online: https://www.photonics.com/Articles/A_History_of_the_Laser_1960_-_2019/a42279 (accessed on 4 June 2021).
122. Slusher, R.E. Laser technology. *Rev. Mod. Phys.* **1999**, *71*, S471–S479. [CrossRef]
123. Warren-smith, S.C.; Sinchenko, E.; Stoddart, P.R.; Monro, T.M. Core Microstructured Optical Fiber. *IEEE Photonics Technol. Lett.* **2010**, *22*, 1385–1387. [CrossRef]
124. Flusberg, B.A.; Cocker, E.D.; Piyawattanametha, W.; Jung, J.C.; Eunice, L.; Cheung, M.; Schnitzer, M.J. Fiber optic imaging. *Nat. Methods* **2010**, *2*, 941–950. [CrossRef]
125. Perales, M.; Wu, C.-L.; Yang, M. Merits of a hybrid fluorescent fiber sensor and power over fiber partial discharge detection solution. In Proceedings of the Fiber Optic Sensors and Applications XV, Orlando, FL, USA, 15–19 April 2018; Volume 10654, p. 5. [CrossRef]
126. Emory, J.M.; Peng, Z.; Young, B.; Hupert, M.L.; Rousselet, A.; Patterson, D.; Ellison, B.; Soper, S.A. Design and development of a field-deployable single-molecule detector (SMD) for the analysis of molecular markers. *Analyst* **2012**, *137*, 87–97. [CrossRef]
127. Sabri, N.; Aljunid, S.A.; Salim, M.S.; Fouad, S. Fiber optic sensors: Short review and applications. *Springer Ser. Mater. Sci.* **2015**, *204*, 299–311. [CrossRef]
128. Zhao, Y.; Hu, X.G.; Hu, S.; Peng, Y. Applications of fiber-optic biochemical sensor in microfluidic chips: A review. *Biosens. Bioelectron.* **2020**, *166*, 112447. [CrossRef]
129. Zhang, L.; Wang, C.; Chen, Y. Development and performance evaluation of portable 405 nm laser-induced fluorescence detector. In Proceedings of the Optics in Health Care and Biomedical Optics X, Online, 11–16 October 2020; Volume 11553, p. 67. [CrossRef]
130. Skinner, C.D. A PDMS sheath flow cuvette for high-sensitivity LIF measurements in CE. *Electrophoresis* **2009**, *30*, 372–378. [CrossRef]
131. Maheedhar, K.; Vidyasagar, M.; Vadhiraja, B.; Fernandes, D.J. Journal of Cancer and Treatment Protein Profile Studies of Cervical Tissue Homogenates Using HPLC-LIF. *Int. J. Cancer Treat.* **2018**, *1*, 47–52.

132. Nguyen, B.T.; Kang, M.J. Application of capillary electrophoresis with laser-induced fluorescence to immunoassays and enzyme assays. *Molecules* **2019**, *24*, 1977. [[CrossRef](#)] [[PubMed](#)]
133. Kamei, T. Laser-induced fluorescence detection modules for point-of-care microfluidic biochemical analysis. *Procedia Eng.* **2011**, *25*, 709–712. [[CrossRef](#)]
134. Xiao, H.; Li, X.; Zou, H.; Yang, L.; Wang, Y.; Wang, H.; Le, X.C.; Zou, H. CE-LIF coupled with flow cytometry for high-throughput quantitation of fluorophores in single intact cells. *Electrophoresis* **2006**, *27*, 3452–3459. [[CrossRef](#)] [[PubMed](#)]
135. Hawthorne, S.B.; St Germain, R.W.; Azzolina, N.A. Laser-induced fluorescence coupled with solid-phase microextraction for in situ determination of PAHs in sediment pore water. *Environ. Sci. Technol.* **2008**, *42*, 8021–8026. [[CrossRef](#)] [[PubMed](#)]
136. Patil, A.; Choudhari, K.S.; Prabhu, V.; Unnikrishnan, V.K.; Bhat, S.; Pai, K.M.; Kartha, V.B.; Santhosh, C. Highly Sensitive High Performance Liquid Chromatography-Laser Induced Fluorescence for Proteomics Applications. *ISRN Spectrosc.* **2012**, *2012*, 1–9. [[CrossRef](#)]
137. Dada, O.O.; Hüge, B.J.; Dovichi, N.J. Simplified sheath flow cuvette design for ultrasensitive laser induced fluorescence detection in capillary electrophoresis. *Analyst* **2012**, *137*, 3099–3101. [[CrossRef](#)]
138. EPA Office of Research and Development. *Site Characterization and Analysis Penetrometer System (SCAPS)*; EPA: Washington, DC, USA, 1995.
139. Davis, W.M.; Cespedes, E.R.; Lee, L.T.; Powell, J.F.; Goodson, R.A. Rapid delineation of subsurface petroleum contamination using the site characterization and analysis penetrometer system. *Environ. Geol.* **1997**, *29*, 228–237. [[CrossRef](#)]
140. Laser-Induced Fluorescence (LIF). Available online: <http://www.cpeo.org/techtree/ttdescript/lasinfl.htm> (accessed on 27 June 2021).
141. Palombi, L.; Raimondi, V. A Compact LIF Spectrometer for in-Field Operation in Polar Environments. *Sensors* **2021**, *21*, 1729. [[CrossRef](#)] [[PubMed](#)]
142. Laserglow Technologies. Available online: <https://www.laserglow.com> (accessed on 27 June 2021).
143. Fu, X.; Li, G.; Dong, D. Improving the Detection Sensitivity for Laser-Induced Breakdown Spectroscopy: A Review. *Front. Phys.* **2020**, *8*, 1–11. [[CrossRef](#)]
144. Goueguel, C.; Laville, S.; Loudyi, H.; Chaker, M.; Sabsabi, M.; Vidal, F. Detection of lead in brass by laser-induced breakdown spectroscopy combined with laser-induced fluorescence. In Proceedings of the Photonics North, Montréal, QC, Canada, 2–4 June 2008; Volume 7099, p. 709927. [[CrossRef](#)]
145. Hilbk-Kortenbruck, F.; Noll, R.; Wintjens, P.; Falk, H.; Becker, C. Analysis of heavy metals in soils using laser-induced breakdown spectrometry combined with laser-induced fluorescence. *Spectrochim. Acta Part B At. Spectrosc.* **2001**, *56*, 933–945. [[CrossRef](#)]
146. Nagli, L.; Gaft, M. Combining laser-induced breakdown spectroscopy with molecular laser-induced fluorescence. *Appl. Spectrosc.* **2016**, *70*, 585–592. [[CrossRef](#)]
147. Tang, Z.; Zhou, R.; Hao, Z.; Ma, S.; Zhang, W.; Liu, K.; Li, X.; Zeng, X.; Lu, Y. Micro-destructive analysis with high sensitivity using double-pulse resonant laser-induced breakdown spectroscopy. *J. Anal. At. Spectrom.* **2019**, *34*, 1198–1204. [[CrossRef](#)]
148. Zhang, D.; Gao, Q.; Li, B.; Liu, J.; Li, Z. Ammonia measurements with femtosecond laser-induced plasma spectroscopy. *Appl. Opt.* **2019**, *58*, 1210. [[CrossRef](#)]
149. Fontana, F.F.; Tassios, S.; Stromberg, J.; Tiddy, C.; van der Hoek, B.; Uvarova, Y.A. Integrated laser-induced breakdown spectroscopy (LIBS) and multivariate wavelet tessellation: A new, rapid approach for lithochemical analysis and interpretation. *Minerals* **2021**, *11*, 312. [[CrossRef](#)]
150. Li, J.; Hao, Z.; Zhao, N.; Zhou, R.; Yi, R.; Tang, S.; Guo, L.; Li, X.; Zeng, X.; Lu, Y. Spatially selective excitation in laser-induced breakdown spectroscopy combined with laser-induced fluorescence. *Opt. Express* **2017**, *25*, 4945. [[CrossRef](#)]
151. Li, J.; Guo, L.; Zhao, N.; Yang, X.; Yi, R.; Li, K.; Zeng, Q.; Li, X.; Zeng, X.; Lu, Y. Determination of cobalt in low-alloy steels using laser-induced breakdown spectroscopy combined with laser-induced fluorescence. *Talanta* **2016**, *151*, 234–238. [[CrossRef](#)] [[PubMed](#)]
152. Li, Q.; Zhang, W.; Tang, Z.; Zhou, R.; Yan, J.; Zhu, C.; Liu, K.; Li, X.; Zeng, X. Determination of uranium in ores using laser-induced breakdown spectroscopy combined with laser-induced fluorescence. *J. Anal. At. Spectrom.* **2020**, *35*, 626–631. [[CrossRef](#)]
153. Yi, R.; Li, J.; Yang, X.; Zhou, R.; Yu, H.; Hao, Z.; Guo, L.; Li, X.; Zeng, X.; Lu, Y. Spectral Interference Elimination in Soil Analysis Using Laser-Induced Breakdown Spectroscopy Assisted by Laser-Induced Fluorescence. *Anal. Chem.* **2017**, *89*, 2334–2337. [[CrossRef](#)] [[PubMed](#)]
154. Li, J.; Zhu, Z.; Zhou, R.; Zhao, N.; Yi, R.; Yang, X.; Li, X.; Guo, L.; Zeng, X.; Lu, Y. Determination of Carbon Content in Steels Using Laser-Induced Breakdown Spectroscopy Assisted with Laser-Induced Radical Fluorescence. *Anal. Chem.* **2017**, *89*, 8134–8139. [[CrossRef](#)]
155. Gravel, J.-F.; Boudreau, D. Laser-Based Detection of Atmospheric Halocarbons. *Rev. Fluoresc.* **2006**, *2007*, 421–443. [[CrossRef](#)]
156. Hitachi Vulcan Handheld Metal Analyzer. Available online: <https://verichek.net/product/hitachi-vulcan-handheld-metal-analyzer> (accessed on 27 June 2021).
157. Rehse, S.J. A review of the use of laser-induced breakdown spectroscopy for bacterial classification, quantification, and identification. *Spectrochim. Acta Part B At. Spectrosc.* **2019**, *154*, 50–69. [[CrossRef](#)]
158. Hellmér, M.; Paxéus, N.; Magnius, L.; Enache, L.; Arnholm, B.; Johansson, A.; Bergström, T.; Norder, H. Detection of pathogenic viruses in sewage provided early warnings of hepatitis A virus and norovirus outbreaks. *Appl. Environ. Microbiol.* **2014**, *80*, 6771–6781. [[CrossRef](#)]

159. Corpuz, M.V.A.; Buonerba, A.; Vigliotta, G.; Zarra, T.; Ballesteros, F.; Campiglia, P.; Belgiorno, V.; Korshin, G.; Naddeo, V. Viruses in wastewater: Occurrence, abundance and detection methods. *Sci. Total Environ.* **2020**, *745*, 140910. [CrossRef]
160. Brahim Belhaouari, D.; Wurtz, N.; Grimaldier, C.; Lacoste, A.; Pires de Souza, G.A.; Penant, G.; Hannat, S.; Baudoin, J.P.; La Scola, B. Microscopic observation of sars-like particles in rt-qpcr sars-cov-2 positive sewage samples. *Pathogens* **2021**, *10*, 516. [CrossRef]
161. Ottawa public health.ca Measuring SARS-CoV-2 RNA (or Measuring COVID-19 Indicators) in Wastewater as an Early Indicator to Help Determine COVID-19 Activity in the Community. Available online: https://www.ottawapublichealth.ca/en/reports-research-and-statistics/Wastewater_COVID-19_Surveillance.aspx (accessed on 30 June 2021).
162. Coker, V.S. *Nanoscience: Volume 1: Nanostructures through Chemistry*; O'Brien, P., Ed.; SPR—Nanoscience; The Royal Society of Chemistry: London, UK, 2012; ISBN 978-1-84973-435-6.
163. Friedman, A.; Claypool, S.; Liu, R. The Smart Targeting of Nanoparticles. *Curr. Pharm. Des.* **2013**, *19*, 6315–6329. [CrossRef]
164. Razzaque, S.; Hussain, S.Z.; Hussain, I.; Tan, B. Design and utility of metal/metal oxide nanoparticles mediated by thioether end-functionalized polymeric ligands. *Polymers* **2016**, *8*, 156. [CrossRef]
165. Taman, R.; Ossman, M.E.; Mansour, M.S.; Farag, H.A. Metal Oxide Nano-particles as an Adsorbent for Removal of Heavy Metals. *J. Adv. Chem. Eng.* **2015**, *5*, 1–8. [CrossRef]
166. Behzadi, S.; Serpooshan, V.; Tao, W.; Hamaly, M.A.; Mahmoud, Y.; Dreaden, E.C.; Brown, D.; Alkilany, A.M.; Omid, C.; Mahmoudi, M. Cellular Uptake of Nanoparticles: Journey Inside the Cell. *Chem. Soc. Rev.* **2018**, *46*, 4218–4244. [CrossRef]
167. Nikolova, M.P.; Chavali, M.S. Metal oxide nanoparticles as biomedical materials. *Biomimetics* **2020**, *5*, 27. [CrossRef]
168. De, A.; Ghosh, S.; Chakrabarti, M.; Ghosh, I.; Banerjee, R.; Mukherjee, A. Effect of low-dose exposure of aluminium oxide nanoparticles in Swiss albino mice: Histopathological changes and oxidative damage. *Toxicol. Ind. Health* **2020**, *36*, 567–579. [CrossRef]
169. Bratovic, A. Synthesis, Characterization, applications, and toxicity of lead oxide nanoparticles. In *Lead Chemistry*; IntechOpen: London, UK, 2020.
170. Saxena, P.; Sangela, V. Harish Toxicity evaluation of iron oxide nanoparticles and accumulation by microalgae *Coelastrella terrestris*. *Environ. Sci. Pollut. Res.* **2020**, *27*, 19650–19660. [CrossRef] [PubMed]
171. Kehrer, J.P. Free Radicals as Mediators of Tissue Injury and Disease. *Crit. Rev. Toxicol.* **1993**, *23*, 21–48. [CrossRef]
172. Slavin, Y.N.; Asnis, J.; Häfeli, U.O.; Bach, H. Metal nanoparticles: Understanding the mechanisms behind antibacterial activity. *J. Nanobiotechnol.* **2017**, *15*, 1–20. [CrossRef] [PubMed]
173. Sengul, A.B.; Asmatulu, E. Toxicity of metal and metal oxide nanoparticles: A review. *Environ. Chem. Lett.* **2020**, *18*, 1659–1683. [CrossRef]
174. Pink, M.; Verma, N.; Schmitz-Spanke, S. Benchmark dose analyses of toxic endpoints in lung cells provide sensitivity and toxicity ranking across metal oxide nanoparticles and give insights into the mode of action. *Toxicol. Lett.* **2020**, *331*, 218–226. [CrossRef] [PubMed]
175. Ramchandran, V.; Gernand, J.M. Examining the in vivo pulmonary toxicity of engineered metal oxide nanomaterials using a genetic algorithm-based dose-response-recovery clustering model. *Comput. Toxicol.* **2020**, *13*, 100113. [CrossRef]
176. Vakili-Ghartavol, R.; Momtazi-Borojeni, A.A.; Vakili-Ghartavol, Z.; Aiyelabegan, H.T.; Jaafari, M.R.; Rezayat, S.M.; Arbab Bidgoli, S. Toxicity assessment of superparamagnetic iron oxide nanoparticles in different tissues. *Artif. Cells Nanomed. Biotechnol.* **2020**, *48*, 443–451. [CrossRef]
177. El Bialy, B.E.; Hamouda, R.A.; Eldaim, M.A.A.; El Ballal, S.S.; Heikal, H.S.; Khalifa, H.K.; Hozzein, W.N. Comparative toxicological effects of biologically and chemically synthesized copper oxide nanoparticles on mice. *Int. J. Nanomed.* **2020**, *15*, 3827–3842. [CrossRef]
178. Halder, A.K.; Melo, A.; Cordeiro, M.N.D.S. A unified in silico model based on perturbation theory for assessing the genotoxicity of metal oxide nanoparticles. *Chemosphere* **2020**, *244*, 125489. [CrossRef]
179. Zhang, H.; Shi, J.; Su, Y.; Li, W.; Wilkinson, K.J.; Xie, B. Acute toxicity evaluation of nanoparticles mixtures using luminescent bacteria. *Environ. Monit. Assess.* **2020**, *192*, 1–8. [CrossRef]
180. Długosz, O.; Szostak, K.; Staroń, A.; Pulit-Prociak, J.; Banach, M. Methods for reducing the toxicity of metal and metal oxide NPs as biomedicine. *Materials* **2020**, *13*, 279. [CrossRef]
181. Sudhakaran, S.; Athira, S.S.; Varma, H.K.; Mohanan, P.V. Determination of the bioavailability of zinc oxide nanoparticles using ICP-AES and associated toxicity. *Colloids Surf. B Biointerfaces* **2020**, *188*, 110767. [CrossRef]
182. Abdussalam-Mohammed, W. Comparison of Chemical and Biological Properties of Metal Nanoparticles (Au, Ag), with Metal Oxide Nanoparticles (ZnO-NPs) and their Applications. *Adv. J. Chem. A* **2020**, *3*, 192–210. [CrossRef]
183. Garcia-Fernandez, J.; Turiel, D.; Bettmer, J.; Jakubowski, N.; Panne, U.; García, L.R.; Llopis, J.; González, C.S.; Montes-Bayón, M. In vitro and in situ experiments to evaluate the biodistribution and cellular toxicity of ultrasmall iron oxide nanoparticles potentially used as oral iron supplements. *Nanotoxicology* **2020**, *14*, 388–403. [CrossRef]
184. Oliveira, E.M.N.; Selli, G.I.; von Schmude, A.; Miguel, C.; Laurent, S.; Vianna, M.R.M.; Papaléo, R.M. Developmental toxicity of iron oxide nanoparticles with different coatings in zebrafish larvae. *J. Nanopart. Res.* **2020**, *22*, 1–16. [CrossRef]
185. Feng, Y.; Chang, Y.; Xu, K.; Zheng, R.; Wu, X.; Cheng, Y.; Zhang, H. Safety-by-Design of Metal Oxide Nanoparticles Based on the Regulation of their Energy Edges. *Small* **2020**, *16*, 1–10. [CrossRef]
186. Mileyeva-Biebesheimer, O. *An Investigation into Metal Oxide Nanoparticle Toxicity to Bacteria in Environmental Systems Using Fluorescence Based Assays*; The University of Toledo: Toledo, OH, USA, 2011.

187. Cao, M.; Cao, C.; Liu, M.; Wang, P.; Zhu, C. Selective fluorometry of cytochrome c using glutathione-capped CdTe quantum dots in weakly basic medium. *Microchim. Acta* **2009**, *165*, 341–346. [[CrossRef](#)]
188. Alsudir, S.; Lai, E.P.C. Selective detection of ZnO nanoparticles in aqueous suspension by capillary electrophoresis analysis using dithiothreitol and L-cysteine adsorbates. *Talanta* **2017**, *169*, 115–122. [[CrossRef](#)]
189. Togashi, D.M.; Ryder, A.G.; McMahon, D.; Dunne, P.; McManus, J. Fluorescence study of bovine serum albumin and Ti and Sn oxide nanoparticles interactions. In Proceedings of the Diagnostic Optical Spectroscopy in Biomedicine IV, Munich, Germany, 17–21 June 2007. [[CrossRef](#)]
190. Cheng, Y.H.; Lai, C.M.; Lin, K.S.; Wang, S.S.S. Effects of metal oxide nanoparticles on the structure and activity of lysozyme. *Colloids Surf. B Biointerfaces* **2017**, *151*, 344–353. [[CrossRef](#)] [[PubMed](#)]
191. Abraham, S. Spectroscopic Studies of Interaction of Protein with Cerium Oxide Nanoparticles. *Asian J. Chem.* **2018**, *30*, 1269–1272. [[CrossRef](#)]
192. Wang, L.; Huang, Z.; Liu, Y.; Wu, J.; Liu, J. Fluorescent DNA Probing Nanoscale MnO₂: Adsorption, Dissolution by Thiol, and Nanozyme Activity. *Langmuir* **2018**, *34*, 3094–3101. [[CrossRef](#)]
193. Liu, B.; Ma, L.; Huang, Z.; Hu, H.; Wu, P.; Liu, J. Janus DNA orthogonal adsorption of graphene oxide and metal oxide nanoparticles enabling stable sensing in serum. *Mater. Horiz.* **2018**, *5*, 65–69. [[CrossRef](#)]
194. Liu, B.; Liu, J. Comprehensive Screen of Metal Oxide Nanoparticles for DNA Adsorption, Fluorescence Quenching, and Anion Discrimination. *ACS Appl. Mater. Interfaces* **2015**, *7*, 24833–24838. [[CrossRef](#)]
195. Ruedas-Rama, M.J.; Walters, J.D.; Orte, A.; Hall, E.A.H. Fluorescent nanoparticles for intracellular sensing: A review. *Anal. Chim. Acta* **2012**, *751*, 1–23. [[CrossRef](#)]
196. Wolfbeis, O.S. An overview of nanoparticles commonly used in fluorescent bioimaging. *Chem. Soc. Rev.* **2015**, *44*, 4743–4768. [[CrossRef](#)] [[PubMed](#)]
197. Basuki, J.S.; Duong, H.T.T.; Macmillan, A.; Erlich, R.B.; Esser, L.; Akerfeldt, M.C.; Whan, R.M.; Kavallaris, M.; Boyer, C.; Davis, T.P. Using fluorescence lifetime imaging microscopy to monitor theranostic nanoparticle uptake and intracellular doxorubicin release. *ACS Nano* **2013**, *7*, 10175–10189. [[CrossRef](#)] [[PubMed](#)]
198. Boreham, A.; Brodewolf, R.; Walker, K.; Haag, R.; Alexiev, U. Time-resolved fluorescence spectroscopy and fluorescence lifetime imaging microscopy for characterization of Dendritic polymer nanoparticles and applications in Nanomedicine. *Molecules* **2017**, *22*, 17. [[CrossRef](#)]
199. Dutta, R.K.; Pandey, A.C. Fluorescent Magnetic Gadolinium Oxide Nanoparticles for Biomedical Applications. *Nanosci. Technol.* **2015**, *2*, 1–6.
200. Wei, H.; Cleary, Z.; Park, S.; Senevirathne, K.; Eilers, H. Fluorescence lifetime modification in Eu:Lu₂O₃ nanoparticles in the presence of silver nanoparticles. *J. Alloys Compd.* **2010**, *500*, 96–101. [[CrossRef](#)]
201. Acikgoz, S.; Ulusu, Y.; Akin, S.; Sonmezoglu, S.; Gokce, I.; Inci, M.N. Photoinduced electron transfer mechanism between green fluorescent protein molecules and metal oxide nanoparticles. *Ceram. Int.* **2014**, *40*, 2943–2951. [[CrossRef](#)]
202. Scalia, G.; Scheffold, F. Lifetime of fluorescent dye molecules in dense aqueous suspensions of polystyrene nanoparticles. *Opt. Express* **2015**, *23*, 29342. [[CrossRef](#)]
203. Dryza, V.; Bieske, E.J. Does the triphenylamine-based D35 dye sensitizer form aggregates on metal-oxide surfaces? *J. Photochem. Photobiol. A Chem.* **2015**, *302*, 35–41. [[CrossRef](#)]
204. Hahm, J.I. Zinc oxide nanomaterials for biomedical fluorescence detection. *J. Nanosci. Nanotechnol.* **2014**, *14*, 475–486. [[CrossRef](#)]
205. Venkatesan, G.; Vijayaraghavan, R.; Chakravarthula, S.N.; Sathiyam, G. Fluorescent zinc oxide nanoparticles of Boswellia ovalifoliolata for selective detection of picric acid. *Front. Res. Today* **2019**, *2*, 2002. [[CrossRef](#)]
206. Kokot, B.; Kokot, H.; Umek, P.; van Midden, K.P.; Pajk, S.; Gravas, M.; Eggeling, C.; Koklic, T.; Urbancic, I.; Strancar, J. Controlled Fluorescent Labelling of Metal Oxide Nanoparticles for Artefact-free Live Cell Microscopy. *bioRxiv* **2021**. [[CrossRef](#)]
207. Zhou, X.; Pu, H.; Sun, D.W. DNA functionalized metal and metal oxide nanoparticles: Principles and recent advances in food safety detection. *Crit. Rev. Food Sci. Nutr.* **2021**, *61*, 2277–2296. [[CrossRef](#)]
208. Velu, R.; De Rosa, M.C. Lateral flow assays for Ochratoxin A using metal nanoparticles: Comparison of “adsorption-desorption” approach to linkage inversion assembled nano-aptasensors (LIANA). *Analyst* **2018**, *143*, 4566–4574. [[CrossRef](#)] [[PubMed](#)]
209. Honda, R.J.; Keene, V.; Daniels, L.; Walker, S.L. Removal of TiO₂ Nanoparticles During Primary Water Treatment: Role of Coagulant Type, Dose, and Nanoparticle Concentration. *Environ. Eng. Sci.* **2014**, *31*, 127–134. [[CrossRef](#)] [[PubMed](#)]
210. Prikryl, J.; Foret, F. Fluorescence detector for capillary separations fabricated by 3D printing. *Anal. Chem.* **2014**, *86*, 11951–11956. [[CrossRef](#)]